



HAL
open science

Tissue mimetic hyaluronan bioink containing collagen fibers with controlled orientation modulating cell migration and alignment

Andrea Schwab, Christophe H elary, Robert Geoffrey Richards, Mauro Alini, David Eglin, Matteo d'Este

► To cite this version:

Andrea Schwab, Christophe H elary, Robert Geoffrey Richards, Mauro Alini, David Eglin, et al.. Tissue mimetic hyaluronan bioink containing collagen fibers with controlled orientation modulating cell migration and alignment. *Materials Today Bio*, In press, 10.1016/j.mtbio.2020.100058 . hal-02862571

HAL Id: hal-02862571

<https://hal.sorbonne-universite.fr/hal-02862571>

Submitted on 9 Jun 2020

HAL is a multi-disciplinary open access archive for the deposit and dissemination of scientific research documents, whether they are published or not. The documents may come from teaching and research institutions in France or abroad, or from public or private research centers.

L'archive ouverte pluridisciplinaire **HAL**, est destin ee au d ep ot et  a la diffusion de documents scientifiques de niveau recherche, publi es ou non,  emanant des  tablissements d'enseignement et de recherche fran ais ou  trangers, des laboratoires publics ou priv es.

Journal Pre-proof

Tissue mimetic hyaluronan bioink containing collagen fibers with controlled orientation modulating cell migration and alignment

Andrea Schwab, Christophe Helary, Robert Geoffrey Richards, Mauro Alini, David Eglin, Matteo D'Este



PII: S2590-0064(20)30018-1

DOI: <https://doi.org/10.1016/j.mtbio.2020.100058>

Reference: MTBIO 100058

To appear in: *Materials Today Bio*

Received Date: 7 April 2020

Revised Date: 21 May 2020

Accepted Date: 22 May 2020

Please cite this article as: A. Schwab, C. Helary, R.G. Richards, M. Alini, D. Eglin, M. D'Este, Tissue mimetic hyaluronan bioink containing collagen fibers with controlled orientation modulating cell migration and alignment, *Materials Today Bio*, <https://doi.org/10.1016/j.mtbio.2020.100058>.

This is a PDF file of an article that has undergone enhancements after acceptance, such as the addition of a cover page and metadata, and formatting for readability, but it is not yet the definitive version of record. This version will undergo additional copyediting, typesetting and review before it is published in its final form, but we are providing this version to give early visibility of the article. Please note that, during the production process, errors may be discovered which could affect the content, and all legal disclaimers that apply to the journal pertain.

© 2020 Published by Elsevier Ltd.

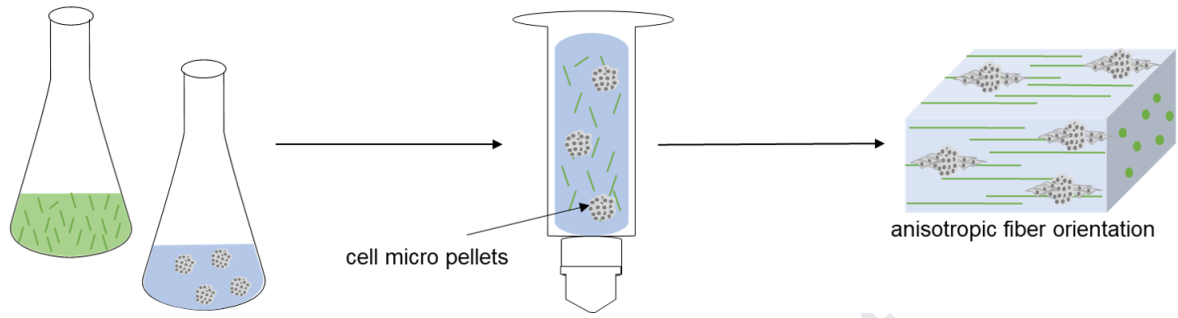
1
2
3
4
5
6
7
8
9
10

Author contribution

Andrea Schwab: Conceptualization, Methodology, Software, Validation, Formal analysis, Investigation, Data Curation, Writing-Original Draft, Reviewing and Editing. **Christophe Hélyary**: Conceptualization, Review and Editing. **Geoff Richards**: Review and Editing, Funding acquisition. **Mauro Alini**: Conceptualization, Review and Editing, Funding acquisition. **David Eglin**: Review and Editing, Project administration, Funding acquisition. **Matteo D'Este**: Conceptualization, Writing-Review and Editing, Supervision, Project administration, Funding acquisition.

Journal Pre-proof

Collagen I / hyaluronan biomaterial for 3D printing



Journal Pre-proof

Tissue mimetic hyaluronan bioink containing collagen fibers with controlled orientation modulating cell migration and alignment.

Andrea Schwab¹, Christophe Helary², Robert Geoffrey Richards¹, Mauro Alini¹, David Eglin¹, Matteo D'Este^{1*}

Author affiliations and contact information

¹ AO Research Institute Davos, Clavadelerstrasse 8, 7270 Davos, Switzerland

² Sorbonne Université | UPMC · Laboratoire de Chimie de la Matière Condensée de Paris (LCMCP), Paris, France

*Corresponding author:

Matteo D'Este

matteo.deste@aofoundation.org

Clavadelerstrasse 8, 7270 Davos, Switzerland

1 Abstract

2 Biofabrication is providing scientists and clinicians the ability to produce engineered tissues
3 with desired shapes, and gradients of composition and biological cues. Typical resolutions
4 achieved with extrusion-based bioprinting are at the macroscopic level. However, for
5 capturing the fibrillar nature of the extracellular matrix (ECM), it is necessary to arrange ECM
6 components at smaller scales, down to the micron and the molecular level.

7 Herein we introduce a bioink containing hyaluronan (HA) as tyramine derivative (THA) and
8 collagen type 1 (Col 1). In this bioink, similarly to connective tissues, Col is present in fibrillar
9 form and HA as viscoelastic space filler. THA was enzymatically crosslinked under mild
10 conditions allowing simultaneous Col fibrillogenesis, thus achieving a homogeneous
11 distribution of Col fibrils within the viscoelastic HA-based matrix. THA-Col composite
12 displayed synergistic properties in terms of storage modulus and shear-thinning, translating
13 into good printability.

14 Shear-induced alignment of the Col fibrils along the printing direction was achieved and
15 quantified via immunofluorescence and second harmonic generation. Cell-free and cell-laden
16 constructs were printed and characterized, analyzing the influence of the controlled
17 microscopic anisotropy on human bone marrow derived mesenchymal stromal cells (hMSC)
18 migration.

19 Anisotropic HA-Col showed cell instructive properties modulating hMSC adhesion,
20 morphology and migration from micro pellets stimulated by the presence and the orientation
21 of Col fibers. Actin filament staining showed that hMSCs embedded into aligned constructs
22 displayed increased cytoskeleton alignment along the fibril direction. Based on gene
23 expression of cartilage/bone markers and ECM production, hMSCs embedded into the
24 isotropic bioink displayed chondrogenic differentiation comparable to standard pellet culture
25 by means of proteoglycan production (Safranin O staining and proteoglycan quantification).

26 The possibility of printing matrix components with control over microscopic alignment brings
27 biofabrication one step closer to capturing the complexity of native tissues.

28

1 Keywords: 3D bioprinting; extracellular matrix; hyaluronan; collagen; cell spheroid;
2 chondrogenesis

3

4 1 Introduction

5 Biofabrication aims at engineering constructs recapitulating the complexity of mammal
6 tissues concerning cell types, chemical and biological gradients, and multiscale architecture.

7 In extrusion-based 3D printing (3DP), the resolution is determined by the size of the nozzle,
8 printing speed and offset, distance between nozzle and printing surface, with resolution
9 ranging from the mm down to the micron range [1]. The physico-chemical properties of the
10 biomaterial and bioink directly influence printing outcome and shape fidelity. The ink is most
11 often a viscoelastic shear-thinning hydrogel (precursor) with good elasticity recovery after
12 high shear and rapid gelation after extrusion [2-4]. In 3DP, resolution is typically referred to
13 the macroscopic architecture of the printed construct rather than on the microscopic features
14 within the printed filaments.

15 By combining different biomaterial ink compositions, gradients of material composition and
16 cellular distribution can be produced using 3D printing techniques [5-7]. Despite impressive
17 advances in the design of bioinks and the printing of complex structures, the field still lacks
18 reliable methods to mimic tissue architectures not only by replicating the ECM composition,
19 but also addressing the (macro)molecular organization within the biomaterial ink at (sub-)
20 micron scale lengths, e.g. on fibrillar levels [8]. However, it is well-known how
21 microarchitectural features provide specific and unique properties to natural tissues [9].

22 Col is the most abundant protein in the ECM, where it is found with a hierarchical fibrillar
23 structure ranging from the triple helix at the molecular level, up to the fibrils and fibers on the
24 microscopic level. Col structure, orientation and spatial arrangement are fundamental
25 towards mechanical stability and anisotropic properties of tissues [10]. The network
26 architecture is also crucial to transmit forces to cells via cell-matrix interaction and
27 contributes to the matrix biochemical environment [11, 12].

1 To bring the 3DP technology one step closer to native tissue architectures, it is necessary to
2 capture micro- and nanostructures within macroscopically complex scaffold geometries [13].
3 Microarchitectural properties can be introduced with polymer self-assembling, a process
4 where macromolecules arrange into stable non-covalent structures. Col 1 [14], fibrin [11],
5 cellulose [15] and silk fibroin [16] are the most prominent materials self-assembling into
6 fibrous structures.

7 Most studies printing Col 1 biomaterial inks employ soluble (acidic) and/or non-fibrillar Col 1
8 inks or blended neutralized Col 1 (Col 1 fractions). Printing an acidic or neutral Col 1
9 dispersion (20-40 mg/ml) of swollen Col fibrils with a high viscosity ($>10^3$ P·s at shear rate of
10 0.1 1/s) requires subsequent lyophilization and chemical crosslinking for scaffold stabilization
11 [17]. Neutralized non fibrillar Col 1 (8 mg/ml) was held at low temperature before extrusion
12 and gelation was induced by printing at 37°C [18]. In another study, neutralized Col 1
13 fractions were printed at high concentrations (20-40 mg/ml) and lower temperature (4-15°C)
14 during extrusion printing and gelled within pre warmed media [19].

15 However, only few studies investigated the formation and presence of Col 1 fibers within the
16 printed hydrogel construct and the influence on cell migration [20-22]. Moreover, cell
17 embedding is limited in the above-mentioned approaches either due to the acidic conditions
18 or the post processing. Another drawback of printing neutralized Col 1 is the phase
19 separation of the self-assembled fibrils from the liquid when extruded [22].

20 Hyaluronic acid or hyaluronan (HA) is another abundant ECM component osmotically
21 capable of holding large amounts of water, and thus functioning as a space filler for fibrillar
22 matrix components, thus providing compressive strength through fluid retention [23]. To our
23 knowledge, methods to control the orientation of Col 1 fibers within a viscoelastic HA-based
24 matrix for bio-fabrication has not been addressed before. Col 1 has been attributed cell
25 instructive properties, including inducing cell attachment by providing the cell adhesion ligand
26 tripeptide Arginine, Glycine and Aspartate that promotes cell attachment and migration [24-
27 26]. Case studies as well as clinical studies showed that Col 1 hydrogel provides a suitable
28 3D environment supporting cartilage defect repair [25, 27-30]. Additionally, Col1 displays

1 marked fibrillogenesis, thus allowing printing of the anisotropic features investigated in this
2 paper. Preliminary experiments (not shown) and literature reports pointed out the non-
3 suitability of Col 2 for printing microscopic architecture [31-33].
4 The aim of this study was the development of a THA-Col 1 composite biomaterial ink and the
5 workflow to 3D print it, fabricating constructs with homogeneous composition and controlled
6 Col fibril orientation at the microscopic level. In addition, the impact of the microscopic
7 anisotropy on the migration behavior of the embedded hMSC micro pellets was analyzed by
8 studying the direction of cell migration out of the micro pellets (Fig. 1). In parallel, the
9 chondro-permissive properties of isotropic THA-Col 1 was investigated. To this aim, the
10 tyramine derivative of HA (THA) was employed to form a continuous matrix where solubilized
11 Col 1 was homogeneously dispersed; THA gelation and Col fibrillogenesis occurred without
12 mutual interference. THA was additionally crosslinked with visible light for final shape
13 fixation, thus achieving a uniform THA matrix containing Col fibrils, which were aligned via
14 the shear forces experienced during the extrusion process. Fibril alignment and cytoskeleton
15 orientation were quantified and compared to casted, isotropic constructs. hMSC micro pellets
16 were embedded in isotropic constructs with different compositions of THA and Col to
17 compare their migration direction and chondrogenic differentiation.

18 2 Materials and Methods

19 2.1 Tyramine modified hyaluronic acid (THA) synthesis

20 THA was synthesized as previously described [34]. Briefly, HA (280-290 kDa, 5 mM
21 carboxylic groups, Contipro Biotech S.R.O) was functionalized via 4-(4,6-dimethoxy-1,3,5-
22 triazin-2-yl)-4-mehtylmorpholinium chloride (DMTMM, TDI) amidation with tyramine by mixing
23 with a stoichiometric ratio of 1:1:1. Functionalization was performed for 24h at 37°C. THA
24 was precipitated by dropwise adding Ethanol (96% v/v), isolated with Gooch filter No. 2 and
25 dried. The degree of substitution was 6.6% as determined by absorbance reading at 275 nm
26 (Multiskan™ GO Microplate Spectrophometer, Thermo Fisher Scientific).

27

1 2.2 THA-Col 1 hydrogel preparation

2 THA (25 mg/ml) was reconstituted with minimum Essential Medium alpha (α -MEM, Gibco)
3 supplemented with 10% v/v bovine fetal serum containing peroxidase from horseradish
4 (HRP, Sigma Aldrich) at the specified concentration at 4°C under agitation. THA for turbidity
5 measurement was reconstituted with PBS. Enzymatic crosslinking was initiated by adding
6 hydrogen peroxide (H_2O_2 , Sigma Aldrich) in different concentrations and incubated for 30 min
7 at 37°C. THA-Col 1 composite was prepared by neutralizing Col 1 (5 mg/ml, Collagen I rat
8 tail in 0.2 N acetic acid, Corning) with NaOH and adding to THA before enzymatic
9 crosslinking was initiated. Mixing ratios by volumes of THA (25 mg/ml) with Col 1 (5 mg/ml)
10 as well as H_2O_2 concentrations are given in brackets for all experimental set ups described in
11 the following paragraphs. For cell encapsulation, hMSC micro pellets were resuspended with
12 THA before adding H_2O_2 . Additional light crosslinking using 0.2 mg/ml of Eosin Y as
13 photoinitiator (Sigma Aldrich) was done for all printing experiments and corresponding
14 control groups of casted samples and the cell migration and cell differentiation studies. The
15 second crosslinking mechanisms was needed to stabilize the (printed) structures of the
16 enzymatically crosslinked but still soft hydrogel. Non-aligned constructs were produced by
17 pipetting the hydrogel precursor with a positive displacement pipette (CP1000, inner
18 diameter ID 1.0 mm, Gilson) into custom made silicon molds (6 mm in diameter). Enzymatic
19 crosslinking was performed for all samples for 30 min at 37°C.

20 To characterize the swelling and degradation of isotropic THA-Col 1, macroscopic images
21 were analyzed by measuring the diameter of cylindrical casted hydrogels at day 0 after
22 reaching equilibrium and after 21 days with ImageJ (National Institute of health, NIH).

1 2.3 3D bioprinting of THA-Col

2 An extrusion based bioprinter (3D Discovery™, RegenHU) was used to prepare THA-Col 1
3 (THA 25 mg/ml, 0.3 U/ml HPR, 0.392 mM H₂O₂, 5.0 mg/ml Col 1) anisotropic hydrogels (.25"
4 cylindrical needles, 15G: ID 1.36 mm, 0.2 bar, writing speed 8 mm/s; 18G: ID 0.84 mm,
5 1.6 bar, writing speed 8 mm/s, Nordson EFD) with subsequent light crosslinking (515 nm
6 LED, speed 4 mm/s). Biomaterial and bioink were transferred into 3CC barred (ID 2.3 mm,
7 Nordson) for enzymatic crosslinking (30 min, 37°C), printed with the above-mentioned
8 parameters (20-22°C room temperature) and transferred into culture media (cell embedded
9 hydrogel) or PBS (cell free).

10 A complex microstructure to mimic microarchitecture of Col fibers in articular cartilage was
11 accomplished with CAD Software (RegenHU). Fibrillar structure in the superficial zone (SZ at
12 the surface) was realized by printing 3 layers of parallel lines, whereas the Middle (MZ) and
13 deep zone (DZ) were designed as circular structures to mimic the arch like geometry.

15 2.4 Rheological characterization

16 Viscoelastic properties of the biomaterial inks were analyzed using Anton-Paar MCR-302
17 rheometer with 1° cone-plate geometry and gap distance of 0.049 mm at 20°C. Silicone oil
18 (Sigma Aldrich) was applied to the external border to prevent drying during the
19 measurement. Viscosity was measured with shear rate ranging from 0.01 1/s to 100 1/s
20 (n=2/group) to evaluate shear thinning behavior of the enzymatically crosslinked THA
21 (0.3 U/ml HRP, 0.52 mM H₂O₂), THA-Col 1 (1:1 v/v) and Col 1 in a rotational experiment.

22 Oscillatory tests (amplitude sweep: frequency 1 Hz, amplitude 0.01 - 100% strain; frequency
23 sweep: amplitude 1% strain, frequency 0.01 - 100 Hz, n=2/group) were performed with
24 parallel plate measuring system at 20°C to characterize the elastic modulus of THA and
25 THA-Col 1 at varying polymer concentrations (0.3 U/ml HRP, 0.65 mM H₂O₂).

26

1 2.5 Turbidity measurement

2 Fibrillation of Col 1 was evaluated by absorbance reading at 313 nm at 37°C at 5, 30 and
3 60 min after induction of neutralization of Col 1 and enzymatic gelation (n=2-5
4 samples/group) of freshly prepared materials with a Multiskan™ GO Microplate Spectrometer
5 (Thermo Scientific). When the Col 1 starts to fibrillate the solution turns from transparent to
6 opaque (more turbid) which is associated with an increase in optical density [35-38]. The
7 following solutions were analyzed: neutralized Col 1, acidic Col 1, THA (0.075 U/ml HRP,
8 0.26 mM H₂O₂) and THA-Col 1 (1:1 and 1:2 v/v) composite undergoing enzymatic cross-
9 linking during measurement of Col 1 fibrillogenesis. Temperature was held at 37°C to induce
10 enzymatic crosslinking of THA and stabilize Col 1 fibrillation.

12 2.6 Second harmonic generation (SHG) imaging

13 To visualize Col 1 fibers (0.3 U/ml HRP, 0.52 mM H₂O₂) (1:1 v/v) SHG images were acquired
14 with a MaiTai multi-photon laser equipped confocal microscope (Leica SP8). SHG signal was
15 collected with HyD detector between 437-453 nm (λ_{ex} 880 nm, output power ap 1.7 W).
16 Additionally, transmitted light and autofluorescence signal (510 - 600 nm) was acquired with
17 varying emission wavelength for SHG detector (λ_{em} 420-436 nm and λ_{em} 454-470 nm) to
18 check for the specificity of SHG signal at 437-453 nm. For deep imaging a long-distance
19 objective (25x water-immersion objective) was used to acquire z-stacks with optimal settings
20 for each sample. Image series acquired with Leica Application Suite X software (LAS X,
21 Leica) were processed with ImageJ (NIH).

23 2.7 Cell culture

24 2.7.1 Cell isolation

25 hMSCs were isolated from bone marrow aspirate with full ethical approval (Ethics committee
26 of University of Freiburg Medical Centre - EK-Freiburg: 135/14) as described elsewhere [39].
27 hMSCs were sub-cultured with α -MEM (Gibco) supplemented with 10% v/v Sera Plus bovine

1 serum (PAN Biotech), 100 U/ml Penicillin, 100 ug/ml Streptomycin (Gibco) and 5 ng/ml basic
2 Fibroblast Growth Factor (FGFb, Fitzgerald Industries International) in a humidified
3 atmosphere of 5% CO₂ with media change every second day.

4

5 2.7.2 3D cell migration and viability study

6 In order to analyze directed cell migration within a 3D environment, cell micro pellets, also
7 known as cell aggregates, were embedded into different hydrogels. Cell spheroids were
8 prepared from hMSC (passage 3-4) in ultra-low attachment petri dish (Corning) with α -MEM
9 media supplemented with 10% bovine serum and 100 U/ml Penicillin, 100 ug/ml
10 Streptomycin via self-assembly to form cell aggregates. After 3 days cell aggregates were
11 harvested, centrifuged (5 min, 500 g) and suspended in a minimum volume of culture media
12 to mix with the hydrogel precursor solution before initiating (enzymatic) crosslinking for THA-
13 Col 1 (1:1 v/v) or THA (0.3 U/ml HRP, 0.39 mM H₂O₂) or neutralizing Col 1 at final cell
14 density of 3 Mio/ml and cultured for 8 days. For THA-Col 1 and THA, an additional light
15 crosslinking of printed and casted samples was done at 515 nm.

16 To evaluate cell migration, samples harvested at day 0, 3, and 8 were stained with phalloidin
17 as described in 2.8.1 and fluorescent images were taken for subsequent quantification of
18 migration length and area (n=3-5 micro pellets/timepoint) described in Chapter 2.9.
19 Additionally, embedding of cell micro pellets allowed to analyze the direction of the cell
20 migration.

21 Live and Dead assay was performed during the migration experiment of hMSC micro pellets
22 embedded in THA-Col 1 (0.3 U/ml HRP, 0.39 mM H₂O₂, 1:1 v/v) of 3D printed and casted
23 samples at day 1 and day 6. H₂O₂ concentration was selected in a range known not to be cell
24 toxic [40]. After washing with PBS, samples were incubated with 2 μ M Calcein AM (Sigma
25 Aldrich) and 1 μ M Ethidium homodimer-1 (Sigma Aldrich) for 30 min at 37°C, washed with
26 PBS and imaged using confocal microscope (LSM800, Carl Zeiss). Dead cells were stained
27 with Ethidium homodimer-1 in red (λ_{ex} 561 nm), cytoplasm of living cells was stained with
28 Calcein-AM in green (λ_{ex} 488 nm).

1

2 2.7.3 Chondrogenic differentiation

3 For chondrogenic differentiation, hMSC (passage 2) were seeded in 6 well microwell plate
4 (AggreWell™ 400 plate) at 1.67 Mio/well according to manufacturer's protocol and cultured
5 for 3 days to form cell micro pellets. Chondrogenic media was composed of high glucose
6 Dulbecco's Modified Eagle Medium (DMEM HG, Gibco) supplemented with non-essential
7 amino acids (1% v/v, Gibco), ascorbic acid 2 phosphate (50 ug/ml, Sigma Aldrich),
8 dexamethasone (100 nM, Sigma Aldrich), ITS+ premix (1% v/v, Corning), TGF β 1 (10 ng/ml,
9 Fitzgerald) and antibiotics (10 U/ml Penicillin, 10 ug/ml Streptomycin, Gibco). Cell micro
10 pellets were embedded in THA-Col 1 (0.5 U/ml HRP, 0.65 mM H₂O₂, 5% w/v Col 1, 1:1 v/v)
11 at final cell concentration of 5 Mio/ml hydrogel volume (400,000 cells/scaffold) before
12 enzymatic gelation, additionally light cross linked, and cultured for 21 days with chondrogenic
13 media. Media was changed 3 times a week. For positive control, standard hMSC pellets
14 were prepared by seeding 250,000 hMSCs into each of a 96 V-Bottom well plate (Ratiolab)
15 and cultured under same conditions.

16

17 2.8 Histological processing and staining

18 2.8.1 Actin filament-Col 1 immunofluorescence staining

19 For actin filament staining in combination with Col 1 immunofluorescent staining, printed and
20 casted THA-Col 1 (1:1 v/v) were fixed with 4% neutral buffered formalin (Formafix AG) at
21 room temperature and stored in PBS at 4°C upon staining.

22 Cytoskeletal organization of hMSC migration from cell micro pellets embedded in
23 enzymatically cross linked THA-Col 1 samples (0.3 U/ml HRP, 0.39 mM H₂O₂) were analyzed
24 on day 0 and after 6 days culture with Phalloidin staining to visualize actin filaments.
25 Hydrogels were permeabilized with 0.5% v/v Triton X-100 (Sigma Aldrich) for 10 min at room
26 temperature, blocked with 10% bovine serum (Sera plus) for 30 min and stained with
27 Phalloidin-TRITC (2 μ g/ml, P1951, Sigma Aldrich) for 45 min at room temperature.
28 Immunofluorescence staining for Col 1 was processed directly after phalloidin staining by

1 overnight incubation with primary antibody (COL 1, 1:5,000 dilution with PBST, monoclonal,
2 Sigma Aldrich). Secondary antibody Goat anti mouse, Alexa fluor 488 (Invitrogen, 1:600
3 diluted with PBST) was incubated for 1h. Cell nuclei were stained with DAPI (2 $\mu\text{g}/\text{ml}$, Sigma
4 Aldrich) for 10 min. Samples were washed between every step with Tween-20 (P1379,
5 Sigma Aldrich) 0.1% v/v in PBS and stored in PBS for microscopy.

6 A confocal microscope (LSM800, Carl Zeiss) was used to acquire fluorescence images (25x,
7 40x water-immersion objectives) to visualize Col 1 matrix and cells. Col 1 fibers within the
8 hydrogel matrix were stained in green (λ_{ex} 488 nm), cell cytoskeleton in red (λ_{ex} 561 nm) and
9 cell nuclei were stained with DAPI in blue (λ_{ex} 405 nm). For all samples, z-stack images were
10 acquired for the three single channels and processed with ImageJ (National Institute of
11 health, NIH) to generate 2D z-projection (max intensity) images. Brightness and contrast
12 settings were adjusted to increase contrast of the single channel images. Merged images of
13 single channels were created with the image overlay tool (merge channels) with ImageJ
14 software (NIH). Images of Col 1 stained samples and cytoskeleton were further processed
15 with ImageJ to quantify fiber orientation and direction of migration as described in 2.10.

16

17 2.8.2 Cryo embedding

18 For histological staining, samples were fixed for 30 min with 4% neutral buffered formalin
19 (Formafix AG) at room temperature and stored, washed with PBS and processed with
20 Sucrose (150 mg/ml and 300 mg/ml, Sigma Aldrich) before being embedded in tissue
21 freezing medium (Leica). Samples were cut with a cryostat microtome (HM 500 OM, Zeiss) to
22 8 μm slices and kept at -20°C until processed for histological staining with safranin O-fast
23 green.

24

25 2.8.3 Safranin O-Fast Green staining

26 To stain the proteoglycans in ECM within hydrogel samples and cell pellets, safranin O
27 staining was performed after 21 days of chondrogenic differentiation. Slides were washed
28 with water to remove the cryo-compound and stained with Weigert's Haematoxylin (12min,

1 room temperature, Sigma Aldrich), blued with tap water (10 min), rinsed with deionized water
2 and stained with Fast Green (0.02% w/v, Fluka) for 6 min to visualize collagenous matrix in
3 green/blue. After washing with acetic acid (1%, Fluka) samples were incubated with
4 safranin O (0.1%, 15 min, Polysciences) to stain proteoglycans in red. After washing with
5 deionized water, staining was differentiated with Ethanol (70%, Alcosuisse) and
6 subsequently dehydrated with series of alcohols (ethanol 96%, ethanol absolute, xylene) and
7 cover slipped (Eukitt, Sigma Aldrich). Microscopic evaluation was performed with brightfield
8 microscope (Olympus BX63, Olympus).

9

10 2.9 Quantification of cell migration length and area

11 A sprout morphology tool in ImageJ (NIH) was used to quantify the migration length on
12 phalloidin stained MAX projection images. For bead and sprout detection the mean threshold
13 method was selected with sample specific adjustment of values (Bead detection: blur radius
14 for bead detection 1.0, minimum bead radius 30-110 μm , dilate beads by factor 1.0-2.8;
15 Sprout detection: sprout detection radius 1.0 μm , minimal plexus area 5,000 μm^2 , minimal
16 sprout area 500 μm^2). Migration area was calculated based on resulting black and white
17 mask from Sprout morphology tool results with ROI area measurement. The calculated area
18 includes the area of the cell micro pellets.

19

20 2.10 Evaluation of Col 1 fiber and cytoskeleton alignment

21 2D fast Fourier transform (FFT) of images acquired with SHG and confocal microscopy for
22 Col 1 immunostaining were used for the evaluation of Col 1 fiber alignment. For both
23 microscopic techniques, single channel images at one focus plane were used ($n = 2-3$
24 samples with 3 focus planes at the beginning, center and end of a printed filament) to
25 investigate the homogeneity of alignment at different z-locations within the strut. For
26 quantification of cytoskeleton orientation, MAX projection images of the red channel (561 nm)
27 of $n=4$ micro pellets at day 6 were processed. The Oval profile plug-in in ImageJ (NIH) was
28 chosen for quantitative evaluation of the Col 1 fiber and cytoskeleton orientation as detailed

1 described elsewhere [41, 42]. In brief, single images were processed with ImageJ (NIH)
2 including unsharp mask, FFT processed, rotated 90°C right, a circular selection with radius
3 512 made, oval plug in for radial sum executed with number of points 360. The resulting grey
4 values were normalized to the maximum grey values of each single image and mean values
5 including standard deviation for both, SHG and confocal images, were shown in the bar
6 diagram.

7

8 2.11 Gene expression analysis: Real-Time Quantitative Polymerase Chain 9 Reaction (PCR)

10 Total RNA was isolated from the samples (THA-Col 1, THA-Col 1 MSC and MSC pellet) at
11 day 0, 14 and 21 using TriReagent® (Molecular Research Centre Inc.) following the
12 manufacturers' protocol. RNA quantity was measured with NanoDrop 1000
13 spectrophotometer (Thermo Fischer). cDNA synthesis of 1 µg RNA was performed with Vilo
14 Superscript (Invitrogen) according to the manufacturer's protocol. Reverse transcription was
15 carried out with Thermocycler (Mastercycler gradient, Eppendorf) including a pre-heating at
16 25°C for 10 min, followed by 42°C for 120 min, inactivation of RT for 5 min at 85°C and
17 cooling down to 4°C.

18 For real time PCR, 10ul of reaction mixture containing TaqMan Universal Master Mix
19 (Thermo Fischer), primer and probes, DEPC water and cDNA was loaded into 384 well
20 plates. PCR was run with an initial heating to 50°C for 2 min, 95°C for 10 min, 40 cycles at
21 95°C for 15 s with the annealing at 60°C for 1 min.

22 Relative gene expression of the chondrogenic associated genes Aggrecan (*ACAN*), Col type
23 2 (*COL2A1*) and *SOX9*, fibrous- and hypertrophy- associated genes Col type 1 and type X
24 (*COL1A1*, *COL10A1*), *RUNX2* as well as the endogenous control ubiquitin C (*UBC*) were
25 calculated using $2^{-\Delta\Delta Cq}$. The *UBC* housekeeping gene has been proven for stability in the
26 present conditions. Two different controls MSC pellets and MSC embedded in THA-Col 1 at
27 day 0 were used for the respective samples. Details on the primers and probe sequence as

1 well as catalogue numbers of Assay-on-Demand (Applied Biosystems) are listed in
2 supplementary (Tab A1).

3

4 2.12 Quantification of Glycosaminoglycans (GAG) and DNA

5 To quantify GAGs and DNA within MSC pellets and cell free and cell laden THA-Col 1
6 hydrogels (n=3 samples/group and time point), samples were digested with Proteinase K
7 (0.5 mg/ml, Sigma Aldrich) at 56°C. DNA content was measured in duplicates using Quant-
8 iTTM PicoGreen (Invitrogen) assay according to the manufacturer's instructions. Fluorescence
9 was measured with a plate reader (Tecan infinite 200 PRO, Tecan) at 485 nm excitation and
10 535 nm emission including a DNA standard curve. The amount of proteoglycans was
11 determined in duplicates by dimethylene blue dye method with absorbance measurement at
12 535 nm including a Chondroitin 4-sulfate sodium salt from bovine trachea (Fluka
13 BioChemika) standard [43]. For calculation of GAGs released into media the cell free THA-
14 Col 1 values were subtracted from the results of hMSC embedded in THA-Col 1.

15

16 2.13 Statistical Analysis

17 All samples were measured in technical duplicates of n = 2-4 biological replicates per group
18 and time point and displayed as box plot including mean value or as mean values with
19 standard deviation. Statistical analysis was performed with Graph Pad Prism (Prism 8, USA).
20 Cell migration length and migration area as well as PCR data was analyzed with multiple t-
21 test. Values of the three sample groups (THA, Col 1 and THA-Col 1) were compared at three
22 time points (day 0, day 3 and day 8) and corrected for multiple comparisons using Holm-
23 Sidak method. Normalization of GAG to DNA values were evaluated using two-way Anova
24 (comparing means of each sample between day 0 and day 21 and between samples at the
25 two time points) with Sidak post hoc test to correct for multiple comparisons. Statistical
26 significance was assumed for p-values <0.05.

27

1 3 Results

2 3.1 Morphology and mechanical properties of the composite network

3 THA-Col 1 composites were prepared dispersing Col 1 into THA, with fibrillogenesis induced
4 by the pH rise and THA crosslinking triggered by H₂O₂ addition and incubation at 37°C. The
5 presence of Col 1 fibers in THA-Col 1 composite hydrogels was characterized by three
6 independent techniques: SHG imaging, confocal microscopy, and turbidimetry (Fig. 2). As
7 positive control Col 1 hydrogel was included for all measurements. The turbidity
8 measurement allowed evaluating the fibrillogenesis kinetics (Fig. 2 E). An increase in
9 absorbance (313 nm) over time was observed ranging from 0.4 to 0.8 for THA 1:1 Col 1 and
10 from 0.06 to 1.3 for THA 1:2 Col 1, indicative of Col 1 fibrillation within the composite. The
11 maximum absorbance values increased with the Col 1 content within the materials, with the
12 highest values around 1.5 absorbance units for the neutralized Col 1 positive control, which
13 was fibrillar from the beginning of the measurement. After 30 minutes of incubation at 37°C a
14 plateau was reached for all groups. Pure Col 1 in acidic and in neutralized solution, and THA
15 showed constant values in turbidity assay without change in absorbance values over time.
16 The fibrillation of Col 1 was further corroborated by imaging techniques. Both, SHG imaging
17 (Fig. 2 C and D) and confocal microscopy of Col 1 immunofluorescent stained samples (Fig.
18 2 A and B), showed obvious presence of Col 1 fibers with a homogenous distribution within
19 THA. Fiber morphology was visibly different, with a thinner and a denser fiber network in
20 THA-Col 1 compared to Col 1 control. Quantification of fibril size and distribution was not
21 possible since the fibrils cross different focal planes resulting in non-reliable values. Images
22 acquired with confocal and SHG microscopy illustrate identical trend in fibrillar
23 characteristics.

24 HRP concentration, H₂O₂ content and mixing ratios of THA and Col 1 were selected based
25 on the requirements for rheological properties and extrudability of the biomaterial ink and
26 Col 1 fibrillogenesis. The viscosity curve clearly demonstrated the shear thinning behavior of
27 the biomaterial ink with an overall higher viscosity of 7 kPa·s for THA-Col 1 and 6 kPa·s for

1 THA at 0.01 1/s, and monotonic decrease for increasing shear rates. At a shear rate higher
2 than 50 1/s the viscosity of THA-Col 1 fell below the value for THA. Neutralized Col 1
3 (5 mg/ml) viscosity was overall lower, ranging from 0.13 k Pa·s at 0.01 1/s to 1 Pa·s at 1 1/s.
4 Acidic Col 1 (pH=4) showed an evident reduction in shear-thinning with viscosity ranging
5 from 0.8 Pa·s to 0.6 Pa·s. Therefore, THA-Col 1 retained the shear thinning behavior
6 required for the biomaterial ink extrusion. An increase in storage modulus was observed in
7 the THA-Col 1 composite hydrogel compared to THA (both samples were prepared at the
8 same THA concentration for matching the concentrations of the enzymatic crosslinking
9 agents, Fig. 2 G).

10 The amplitude sweep showed similar profile for THA and THA-Col 1, with the Col 1 presence
11 implicating an increase in storage modulus from 220 Pa to 608 Pa at 0.1% strain, but similar
12 decrease trend at higher strain (Fig. 2 G). This behavior is indicative that THA viscoelastic
13 properties are not disrupted by the formation of the composite with Col 1. Enzymatically and
14 light crosslinked THA-col 1 isotropic samples swelled to 150% to the original diameter to
15 0.89 ± 0.04 cm. No degradation in terms of change in sample diameter occurred in the cell
16 free group during incubation in media at 37°C (0.93 ± 0.04 cm).

17

18 3.2 Cell instructive properties of THA-Col 1 bioink

19 hMSCs micro pellets were embedded into bioink made of THA-Col 1 and into its single
20 components to determine how the composition influences cell attachment and migration from
21 the micro pellets. Fig. 3 A illustrates a panel of MAX projection images stained for actin
22 filaments on day 0, day 3 and day 8. Cells migrated out of the uniformly dispersed micro
23 pellets into the biomaterials in presence of Col 1 (THA-Col 1 and Col 1), whereas no
24 migration was observed in THA hydrogels.

25 Migration length and migration area were quantified with the ImageJ sprout Morphology Tool
26 on MAX projections images stained with phalloidin. Mean values for both parameters confirm
27 the highest migration in Col 1 (migration length: 40165 μm ; migration area: 297 μm^2),
28 followed by THA-Col 1 (migration length: 26964 μm , $p=0.0050$ compared to THA day 3;

1 migration area: $246 \mu\text{m}^2$ $p=0.0720$ compared to THA day 3) on day 3. From day 3 to day 8
2 the migration increased further for Col 1 and THA-Col 1 (THA-Col 1 migration length:
3 $63838 \mu\text{m}$, $p=0.0005$ compared to THA day 8; migration area: $582 \mu\text{m}^2$, $p=0.0001$ compared
4 to THA day 8). In THA, migration area and migration length of hMSC micro pellets remained
5 unvaried for the whole duration of the experiment. Due to significant shrinkage of Col
6 1 hydrogels the quantification of the two parameters on day 8 was not possible for Col 1 (Fig.
7 3 B-C). The differences in spheroid size derived from the variation in focus plane within the
8 3D constructs.

10 3.3 In vitro chondrogenic differentiation

11 Chondrogenic differentiation potential of hMSC micro pellets embedded in isotropic THA-Col
12 1 was compared to hMSC pellet culture as positive control, and was evaluated by qPCR,
13 safranin-O staining and total GAG/DNA content. Gene expression analysis of hMSCs
14 spheroid embedded in THA-Col 1 (Fig. 4 A) showed an increase in chondrogenic related
15 markers *COL2A1* (1,000-10,000 fold), *ACAN* (10-1,000 fold) and *SOX9* (<20 fold) over time,
16 similarly to hMSCs pellet. *COL1A1* was slightly down regulated (0.1 – 1.0-fold), while
17 *COL10A1* showed an increase of up to 100 times for the two groups at day 14. At day 21,
18 *COL10A1* stayed constant for hMSC embedded THA-Col 1 whereas the fold change relative
19 to control sample decreased to <10 for hMSCs pellet. *RUNX2* upregulation was much less
20 pronounced (< 10-fold change) compared to the extracellular matrix associated genes. The
21 ratio *COL2A1/COL1A1* (Fig. 4 B), was higher for hMSC micro pellets embedded in THA-Col
22 1 (day 14: 5353 ± 1699 , $p= 0.0242$ compared to day 0 , day 21: 1650 ± 409 , $p=0.0293$
23 compared to day 0) compared to hMSCs pellet (day 14: 931 ± 568 $p= 0.1467$ compared to
24 day 0, day 21: 300 ± 69 $p= 0.0260$ compared to day 0).

25 At day 21, an increase in proteoglycans resulted for both groups (Fig. 4 C-D). Total amount
26 of GAGs increased from $0.46 \pm 0.38 \mu\text{g/ml}$ to $4.48 \pm 0.13 \mu\text{g/ml}$ ($p<0.0001$) for hMSCs pellet
27 and from $1.18 \pm 0.20 \mu\text{g/ml}$ to $4.48 \pm 0.69 \mu\text{g/ml}$ ($p<0.0001$) for hMSCs micro pellets
28 embedded in the bioink. Release of proteoglycans in the media was $5.88 \pm 0.92 \mu\text{g}$ and

1 13.58 ± 2.93 µg, respectively. Both groups retained around 25% of the total produced
2 proteoglycans within the sample (MSC pellet 26.8%, THA-Col 1 MSC 23.3%). Normalizing
3 total GAG to DNA values in the samples increased for hMSCs pellet within 21 days to 3.88
4 ± 0.42 (p<0.0001) and for hMSCs embedded in THA-Col 1 to 2.34 ± 0.24 (p<0.0001).

5 The histological staining confirmed the chondrogenic differentiation. After 21 days of culture
6 a homogenous distribution of safranin O positive staining was observed for hMSCs pellet and
7 hMSC embedded in THA-Col 1 (Fig. 4 E-F). The hMSC micro pellets were no longer visible
8 in the point of initial seeding because of the migration throughout the whole hydrogel,
9 resulting in a homogenous cell distribution. hMSCs morphology was comparable between
10 the cells in the pellet and the cells embedded in the hydrogel; most cells appeared to be
11 condensed or rounded with a low population of spindle shaped cells at day 21.

12 Overall, this experiment pointed out that hMSC embedded in the isotropic THA-Col 1 bioink
13 is permissive to cell migration, GAG retention and that it retains the same chondrogenic
14 potential as the gold standard pellet culture.

15

16 3.4 3DP to fabricate microscopically anisotropic scaffolds

17 The enzymatic crosslinking of the THA-Col 1 biomaterial ink was optimized in terms of HRP
18 and H₂O₂ concentrations for extrusion printing to meet the requirements of a shear thinning
19 behavior and to be extruded as a homogenous and continuous filament. Printing speed of
20 8 mm/s was found to be optimal for the composite ink for 15G needle and 4 mm/s for 22G,
21 respectively. After optimizing THA-Col 1 biomaterial ink, the Col 1 presence and fibrillar
22 orientation were characterized. SHG imaging and confocal microscopy were used to
23 visualize the Col 1 fibrils in the THA-Col 1 biomaterial ink after extrusion printing. The fibrillar
24 structure of Col 1 in the composite was preserved after printing and resulted in an anisotropic
25 material. Representative microscopic images in Fig. 5 A and C clearly demonstrate the
26 presence of parallel aligned Col 1 fibers along the direction of the printing.

27 To further characterize this property, the ImageJ Oval plug in was used to quantify the
28 alignment of THA-Col 1 after printing and compare to casted THA-Col 1 and casted Col 1.

1 Casted THA-Col 1 resulted in the least anisotropic properties, followed by casted Col 1.
2 Comparing the peak width of the preferred orientation in the printed samples at normalized
3 grey value of 0.5 (SHG: 43 degree, confocal microscopy: 60 degree) to the corresponding
4 casted one (SHG: 115 degree, confocal microscopy: 150 degree) and the casted Col 1
5 (SHG: 62 degree, confocal microscopy: 129 degree) a clear narrowing of the Col 1 fiber
6 orientation dispersity was observed for the printed sample (Fig. 5 B and D).
7 The control over the parallel fiber orientation was used to produce a construct imitating the
8 Col orientation in knee articular cartilage. Fibrillar structure in the superficial zone (SZ at the
9 surface) was realized by printing parallel lines, whereas the Middle (MZ) and deep zone (DZ)
10 by an arch like geometry shown in Fig. 5 E and G with an overall sample size of 1.4 x 1.6 cm.
11 The resolution of the printed sample shown in Figure 5 G ranges on the millimeter scale
12 given by the inner diameter of the needle. Immunofluorescent staining against Col 1 clearly
13 shows the fibrillar alignment in the three zones with horizontal fibers in the SZ, vertical
14 alignment in the DZ and more isotropic appearance in the MZ.

15

16 3.5 Effect of 3DP on cell migration in THA-Col 1 bioink

17 After characterization of the material microstructure and properties, we investigated the
18 response of hMSCs on aligned anisotropic versus isotropic fibers in the THA-Col 1. The
19 bioink was either printed with a cylindrical needle or extruded from the cartridge without
20 needle attached and compared to casted samples. Live/dead staining of hMSC aggregates
21 embedded in THA-Col 1 (printed versus casted) are shown in Fig. 6 A at day 1 and 6. Cells
22 were viable after printing and remained viable over culture time. At day 1, some dead cells
23 (stained in red) were visible mainly in the center of the micro pellets. After 6 days, less dead
24 cells were present compared to day 1 in all three groups. The live/dead staining also showed
25 no toxic effect of the addition of H₂O₂ (0.39 mM) in THA and THA-Col 1 to initiate enzymatic
26 gelation.

27 During *in vitro* culture, hMSC migrated from the micro pellets in all three groups. Observing
28 the cytoskeleton orientation via phalloidin staining, MSCs alignment was more pronounced in

1 the printed groups, while hMSC showed a more isotropic cytoskeletal orientation in the
2 extruded and casted group. The overlay image of actin filament staining (red), and cell nuclei
3 (blue) demonstrated the unidirectional migration of the cells (Fig. 6 B).

4 Fig. 6 C illustrates the orientation of the cytoskeleton based on MAX projection of the red
5 channel. The group printed with a 15G needle (left) displays two clear maxima along the
6 orientation of the Col fibers determined by the printing direction (and the 180° from it),
7 indicated by the green arrows, thus indicating cytoskeleton alignment along the Col fibers.
8 For the group undergoing extrusion without needle (2.4mm diameter, center) the peaks were
9 markedly broadened and more jagged, indicative of a more random distribution; this trend
10 was even more apparent for the casted sample, where the distribution assumes a white
11 noise profile.

12

13 4 Discussion

14 Extrusion-based printing has achieved significant advances in controlling construct
15 resolution, composition and shape. However, control over the microscopic architecture has
16 been mostly overlooked. Mechanical and biological properties of animal tissues depend not
17 only on the chemical composition, but also on the specific spatial arrangement of structural
18 molecules and biological factors [9]. For example, cartilage is composed of a
19 glycosaminoglycan-based matrix containing Col 1 fibers with specific orientation, parallel to
20 the surface on the superficial zone and perpendicular in deeper layers [44].

21 In the present work, we propose a technique to introduce anisotropic properties into a THA-
22 Col 1 composite biomaterial. Having two parallel occurring crosslinking mechanisms, we
23 overcame the difficulty in homogenous mixing Col 1 fibrils into a viscoelastic HA-based
24 matrix by combining a previously developed bioink based on the tyramine derivative of HA
25 [45] with acidic-solubilized Col 1, which was buffered upon mixing, thereby forming fibrils.
26 Since both precursors, THA bioink and Col 1, are in liquid form, mixing to homogeneity was
27 easily achieved, as visualized with microscopic techniques (Fig. 2 A-D). A distinctive

1 advantage of the preparation method here illustrated is that THA crosslinking and Col 1 fibril
2 formation occur simultaneously, thus avoiding phase separation [22]. Although the Col 1
3 fibrils in the confocal and SHG images in Fig. 2 seem to differ between pure Col 1 and THA-
4 Col 1, both casted, there is no difference in fiber diameter as shown by secondary electron
5 and transmission electron microscopy previously [46]. The visual differences can be
6 explained by the MAX projection of several focus plans within the 3D constructs and thus
7 fibers in the deeper regions tend to display smaller fibrils compared to the fibrils captured in
8 z-directions closer to the objective.

9 The preservation of the fibrillar microstructure of low concentrated neutral Col 1 (2.5 mg/ml
10 final concentration in composite) within THA (12.5 mg/ml final concentration) after 3DP is a
11 further feature required to produce the anisotropic microstructure.

12 Casted Col 1 hydrogels have been extensively used in the literature, but the fibrillar structure
13 was not extensively investigated when combined with a second polymer. Binner *et al.*
14 characterized a star shaped poly (ethylene glycol) hydrogel mixed with Fluorescein-
15 isothiocyanate labelled Col 1. Besides a homogenous distribution of the Col 1, no fibrillar
16 structure was shown and further characterized [47]. Formation of Col 1 fibers resulted to be
17 dependent on the incubation time at 4°C prior to pH neutralization and thus inducing
18 fibrillation when combined with Matrigel [48]. A thermally controlled printing of Col 1
19 (6 mg/ml) blended with Pluronic (60% w/v) resulted in Col 1 fiber formation and aggregation
20 with a dependency of the fiber alignment with the amount of media added and thus time to
21 dissolve the Pluronic out of the blend [20].

22 The shear thinning and viscosity behavior of high concentration neutralized Col 1 (20-60
23 mg/ml) has been characterized by different groups [19, 49]. In contrast, 3D printing of
24 neutralized pure Col 1 at low concentrations is challenging due to the lack of shear thinning
25 and shape retention. At the low concentration used in this study (≤ 5 mg/ml), printability was
26 rescued by the shear thinning THA. A similar approach was presented by Duarte Capos *et*
27 *al.* using agarose as shear thinning component [50]. On the other hand, printing properties of
28 THA previously investigated in our group were preserved upon mixing with Col 1 [51].

1 The addition of Col 1 to THA increased the storage modulus. Thus, the fibrillar network within
2 the viscoelastic THA can be used as a design parameter to modulate the mechanical
3 properties. The formation of di-tyramine bonds between Col 1 and THA could be one reason
4 for the synergistic effect [46, 52]. Other advantages of the composite are that the cell-
5 mediated shrinking of Col 1 scaffolds is reduced; on the other side, Col 1 provides cell
6 attachment sites to the HA, and an ECM-mimetic fibrillar matrix. Reduced shrinkage of Col 1
7 was also observed when this natural material was combined with silk when pulmonary
8 fibroblasts were embedded [52].

9 Within the casted gels the fibrils exhibited either random orientation or local domains with
10 some degree of orientation, which could be attributed to the low but non-zero shear forces
11 experienced during casting from a pipette.

12 After 3D printing of the composite, an overall alignment along the printing axis was observed,
13 as expected. Therefore, the low-grade enzymatic crosslinking of the THA preserved at least
14 in part the capability of the fibrils to comply with the shear stimulus when extruded.

15 Shear-induced alignment of fibrils but also molecules has been reported in literature [21, 53-
16 56]. Kim *et al.* controlled the fiber alignment in dependence of the needle diameter during
17 printing showing a higher degree of alignment when using 30G compared to 20G needles
18 [53]. This intuitive behavior was not observed in the present study; rather, with thinner
19 needles the fibrillar structure was disrupted, possibly due to the significantly higher pressure
20 that was needed to achieve extrusion, potentially creating discontinuity or turbulence
21 (supplementary Fig. A1). Moncal *et al.* introduced Col printing (6 mg/ml) with a thermally
22 controlled set-up using Pluronic as sacrificial material and quantified the alignment of Col
23 fibers along printing direction related to the amount of media and incubation time (0-48h) to
24 induce fibrillation but with overall low anisotropy indices [20]. An agarose-Col (5 mg/ml
25 agarose, 2 mg/ml Col 1) blend with equally distributed col fibers but no signs of alignment
26 after printing was presented by Koepf *et al.* [57]. A different approach to align Col 1 fibers
27 was shown by Betsch *et al.* They aligned iron nanoparticle loaded agarose-Col 1 biomaterial
28 ink after exposure to a magnetic field. The alignment was most prevalent in Col 1 (3 mg/ml)

1 compared to the composite (agarose 3 mg/ml, Col 1 2.5 mg/ml) only in the group with
2 magnetic field exposure [58]. Yang *et al.* also used electrically assisted printing to mimic Col
3 1 orientation in meniscus by radial and circumferential aligned carbon nanotubes [59]. With
4 the method here presented, we achieved alignment of Col 1 fibrils within a composite using
5 exclusively natural ECM molecules avoiding using synthetic non-degradable components
6 simply by 3D extrusion printing. Col 1 only can evolve over time becoming isotropic. This
7 behavior is prevented within the composite, due to the presence of gelled THA stabilizing Col
8 1 fibrils.

9 Due to the signs of Col fibril disruption at high shear stresses indicated by less alignment
10 (Fig. A2) and the decrease in storage modulus shown with amplitude sweep (Fig. 2 G), the
11 resolution of the here introduced biomaterial ink is limited. As shown in Fig. A4 the THA-Col
12 1 filaments tend to spread due to its soft properties after enzymatic crosslinking but still
13 allows to create multi-layered crisscross structures at moderate resolution (Supplementary
14 Fig. A4). The more oval instead of rectangular shape of the transversal pore geometry within
15 this printed crisscross structure indicate filament fusion to some extent which was described
16 by Ouyang *et al.* as one indicator of shape fidelity [60]. Although the resolution of the
17 biomaterial ink is lower compared to what can be reached in the field, this had no negative
18 effect on the printing of the construct mimicking the fiber orientation of articular cartilage.

19 The combination of the two ECM components brings biological features and directs cellular
20 behavior. Single cell seeding resulted in enhanced adhesion, overcoming limited cell
21 attachment reported before [51]. Similar results were observed with cell aggregates, where
22 the presence of Col 1 increased the migration length and area. This behavior can be
23 attributed to the presence of the integrin interaction site Arginine, Glycine and Aspartate,
24 (RGD sequence) naturally contained in Col 1 inducing cell adhesion [24]. A direct correlation
25 of cell adhesion and RGD density was shown also for electrospun HA functionalized with
26 RGD peptide by Kim *et al.* [61]. The above cited agarose-Col blend has been shown to
27 enhance smooth muscle cell spreading and attachment and thus confirming that the
28 presence of Col 1 in a composite influences cell spreading [57].

1 The local microstructure of the material but also fiber parameters regulate cell response [62,
2 63]. In this study, hMSC migration was stimulated along the unidirectional orientation of the
3 Col 1 fibers after 3D printing. Due to the interaction of hMSC with the Col 1 fibers, the original
4 orientation of the parallel fiber alignment was less visible in confocal microscopy (Fig. 6 B).
5 However, the overlapping direction of cytoskeleton orientation and fiber alignment were
6 visualized and quantified (supplementary Fig. A2). In a comparable study, Kim *et al.* showed
7 the unidirectional actin filament orientation of keratinocytes embedded in corneal stroma-
8 derived decellularized ECM after printing which were less pronounced in non-printed
9 samples for preparation of corneal implants [53]. Yang *et al.* reported an increase in tendon
10 associated genes of rat MSC with oriented Col 1 fiber membrane compared to the isotropic
11 sample [64]. Whether this observation relies on the anisotropic properties or is partially
12 induced by the shear stress during printing is not fully understood.

13 HA has been attributed a plethora of biological properties, including inducing cell
14 proliferation, chondrogenic differentiation and matrix synthesis [65, 66]. The THA-Col 1
15 composite here proposed supported the migration and chondrogenic differentiation of hMSC
16 micro pellets, resulting in cartilage like matrix deposition throughout the hydrogel. Matrix
17 deposition of hMSCs embedded in THA-Col 1 was uniform, with staining comparable to the
18 standard pellet culture control (Fig. 4 E-F). Importantly, despite Col 1 presence and invasion
19 of the whole matrix, cell morphology was also comparable to the pellet culture, showing a
20 more condensed rather than spindle shape morphology indicating cell differentiation along
21 chondrogenic lineage. Cells within micro pellets are in their preferred 3D condensed
22 environment with high inter cellular contact compared to single cell embedding at high cell
23 density (10-20 Mio/ml) required for *in vitro* chondrogenic differentiation within biomaterials
24 and thus can explain their good pro chondrogenic differentiation within the biomaterial. hMSC
25 migration out of micro pellets embedded in Col hydrogel subjected to *in vitro* chondrogenic
26 differentiation was also reported by Wang *et al.* showing that those cells were positively
27 stained for chondrogenic differentiation markers including Col 1 and 2, aggrecan and SOX9
28 [67]. Good chondrogenic differentiation starting from micro pellets or cell aggregates was

1 reported also by Markway *et al.*, whereas Rogan observed less chondrogenic differentiation
2 compared to the gold standard in the pellet culture [67-69]. The biomaterial used in this study
3 overcomes the limitation of extracellular matrix deposition only in the pericellular region
4 which is attributed to many seminatural materials used for cartilage tissue engineering.
5 One possible concern regarding cartilage regeneration is the use of Col type 1 instead of
6 type 2 for our bioink. Clinical studies of a cell free type 1 Col hydrogel (CaReS-1S[®], Arthro
7 Kinetics AG) implanted in focal, full layer cartilage defects have shown good clinical outcome
8 addressing defect filling and homogenous structure of the repair tissue [28], with the Col 1
9 disappearing *in vivo* to leave space to the cell-deposited Col 2 [30]. In a minipig study
10 colonization of the cell free Col 1 matrix gave outcome comparable to matrix assisted
11 chondrocyte implantation [25, 29]. Jiang *et al.* demonstrated superior chondrogenic
12 differentiation of MSC embedded in Col 1 compared to MSC only in a rat model [70]. On the
13 other hand, HA has been combined with Col 1 or gelatin before with similar outcomes that
14 chondrogenic differentiation is promoted in the composite compared to HA or Col 1 only [71-
15 73].
16 One limitation of the present technique is the shear-induce alignment, limiting the degrees of
17 spatial freedom in fibril arrangement. Another limitation is the missing quantification of the
18 Col 1 fibers within the composite compared to Col 1 hydrogel and how the microstructural
19 alignment affects cell alignment. This was partially due to technical limitations in visualizing
20 Col 1 fibrils crossing different focus planes within a 3D hydrogel and thus dealing with
21 autofluorescence, light scattering and the opaque character of the hydrogel. For further
22 development, the capacity of regenerating cartilage or other tissues should be tested
23 interrogating specifically the effect of the orientation separately from the composition,
24 comparing random oriented or non-fibrillar constructs with aligned constructs.

25

1 5 Conclusions

2 Overall, in this work, we have presented a method to obtain an THA-Col 1 composite with
3 macroscopic homogeneity and microscopic heterogeneity mimicking the macromolecular
4 architecture of native tissues. We achieved a uniform distribution of Col 1 fibers within an
5 HA-based viscoelastic matrix starting from liquid precursors with simultaneous Col 1
6 fibrillation and HA crosslinking. The orientation of the Col 1 fibers in the 3D printed construct
7 was controlled with the shear stress during printing and had a direct impact on cell behavior.
8 The biomaterial ink here introduced can be extended to other fibrillar proteins to produce
9 similar microstructural features. The possibility of printing ECM components with control over
10 microscopic alignment brings biofabrication one step closer to capturing the complexity of
11 biological tissues.

12

13 Author contribution

14 **Andrea Schwab**: Conceptualization, Methodology, Software, Validation, Formal analysis,
15 Investigation, Data Curation, Writing-Original Draft, Reviewing and Editing. **Christophe**
16 **Hélary**: Conceptualization, Review and Editing. **Geoff Richards**: Review and Editing,
17 Funding acquisition. **Mauro Alini**: Conceptualization, Review and Editing, Funding
18 acquisition. **David Eglin**: Review and Editing, Project administration, Funding acquisition.
19 **Matteo D'Este**: Conceptualization, Writing-Review and Editing, Supervision, Project
20 administration, Funding acquisition.

21

22 Declaration of competing interests

23 The authors declare that they have no known competing financial interests or personal
24 relationships that could have appeared to influence the work reported in this paper.

25

26 Data availability

1 The processed data required to reproduce these findings are available to download from
2 Mendeley-Data link <http://dx.doi.org/10.17632/vcxdk7s8jy.1> .

3

4 Acknowledgements

5 This work is part of the osteochondral defect collaborative research program supported by
6 the AO Foundation.

7 This project has been partially supported by "L'Agence Nationale de la Recherche" (ANR)
8 and the Swiss National Science Foundation (SNSF): INDEED project, SNSF's grant number
9 310030E_189310 and ANR's grant number ANR-19-CE06-0028.

10 The authors acknowledge support of the Scientific Center for Optical and Electron
11 Microscopy ScopeM of the Swiss Federal Institute of Technology ETHZ for acquiring SHG
12 images.

13 The Graubünden Innovationsstiftung is acknowledged for its financial support.

14 The authors thank Dr. Christoph Sprecher for his support with confocal microscopy settings
15 and Luca Ambrosio MD for his support setting up the turbidity measurement.

16

17 References

18 [1] S.V. Murphy, A. Atala, 3D bioprinting of tissues and organs, *Nat Biotechnol* 32(8) (2014)
19 773-85.

20 [2] M. Hospodiuk, M. Dey, D. Sosnoski, I.T. Ozbolat, The bioink: A comprehensive review on
21 bioprintable materials, *Biotechnol Adv* 35(2) (2017) 217-239.

22 [3] F.P.W. Melchels, W.J.A. Dhert, D.W. Hutmacher, J. Malda, Development and
23 characterisation of a new bioink for additive tissue manufacturing, *J Mater Chem B* 2(16)
24 (2014) 2282.

25 [4] J. Malda, J. Visser, F.P. Melchels, T. Jungst, W.E. Hennink, W.J. Dhert, J. Groll, D.W.
26 Hutmacher, 25th anniversary article: Engineering hydrogels for biofabrication, *Adv Mater*
27 25(36) (2013) 5011-28.

28 [5] S.M. Bittner, B.T. Smith, L. Diaz-Gomez, C.D. Hudgins, A.J. Melchiorri, D.W. Scott, J.P.
29 Fisher, A.G. Mikos, Fabrication and mechanical characterization of 3D printed vertical

- 1 uniform and gradient scaffolds for bone and osteochondral tissue engineering, *Acta Biomater*
2 90 (2019) 37-48.
- 3 [6] T.J. Klein, S.C. Rizzi, J.C. Reichert, N. Georgi, J. Malda, W. Schuurman, R.W. Crawford,
4 D.W. Hutmacher, Strategies for zonal cartilage repair using hydrogels, *Macromol Biosci*
5 9(11) (2009) 1049-58.
- 6 [7] L.H. Nguyen, A.K. Kudva, N.S. Saxena, K. Roy, Engineering articular cartilage with
7 spatially-varying matrix composition and mechanical properties from a single stem cell
8 population using a multi-layered hydrogel, *Biomaterials* 32(29) (2011) 6946-52.
- 9 [8] M.A. Heinrich, W. Liu, A. Jimenez, J. Yang, A. Akpek, X. Liu, Q. Pi, X. Mu, N. Hu, R.M.
10 Schiffelers, J. Prakash, J. Xie, Y.S. Zhang, 3D Bioprinting: from Benches to Translational
11 Applications, *Small* 15(23) (2019) e1805510.
- 12 [9] P. Datta, V. Vyas, S. Dhara, A.R. Chowdhury, A. Barui, Anisotropy Properties of Tissues:
13 A Basis for Fabrication of Biomimetic Anisotropic Scaffolds for Tissue Engineering, *Journal of*
14 *Bionic Engineering* 16(5) (2019) 842-868.
- 15 [10] M.D. Shoulders, R.T. Raines, Collagen structure and stability, *Annu Rev Biochem* 78
16 (2009) 929-58.
- 17 [11] A. Malandrino, X. Trepate, R.D. Kamm, M. Mak, Dynamic filopodial forces induce
18 accumulation, damage, and plastic remodeling of 3D extracellular matrices, *PLoS Comput*
19 *Biol* 15(4) (2019) e1006684.
- 20 [12] A.D. Doyle, K.M. Yamada, Mechanosensing via cell-matrix adhesions in 3D
21 microenvironments, *Exp Cell Res* 343(1) (2016) 60-66.
- 22 [13] W.M. Han, S.J. Heo, T.P. Driscoll, J.F. Delucca, C.M. McLeod, L.J. Smith, R.L. Duncan,
23 R.L. Mauck, D.M. Elliott, Microstructural heterogeneity directs micromechanics and
24 mechanobiology in native and engineered fibrocartilage, *Nat Mater* 15(4) (2016) 477-84.
- 25 [14] B. Patel, Z. Xu, C.B. Pinnock, L.S. Kabbani, M.T. Lam, Self-assembled Collagen-Fibrin
26 Hydrogel Reinforces Tissue Engineered Adventitia Vessels Seeded with Human Fibroblasts,
27 *Sci Rep* 8(1) (2018) 3294.
- 28 [15] A.S. Gladman, E.A. Matsumoto, R.G. Nuzzo, L. Mahadevan, J.A. Lewis, Biomimetic 4D
29 printing, *Nat Mater* 15(4) (2016) 413-8.
- 30 [16] S.A. Bradner, M. McGill, A. Golding, R. Grudt, D.L. Kaplan, Silk Hydrogel Microfibers for
31 Biomimetic Fibrous Material Design, *Macromol Mat Eng* 304(7) (2019) 1900045.
- 32 [17] A. Lode, M. Meyer, S. Bruggemeier, B. Paul, H. Baltzer, M. Schropfer, C. Winkelmann,
33 F. Sonntag, M. Gelinsky, Additive manufacturing of collagen scaffolds by three-dimensional
34 plotting of highly viscous dispersions, *Biofabrication* 8(1) (2016) 015015.
- 35 [18] N. Diamantides, C. Dugopolski, E. Blahut, S. Kennedy, L.J. Bonassar, High density cell
36 seeding affects the rheology and printability of collagen bioinks, *Biofabrication* 11(4) (2019)
37 045016.

- 1 [19] E.O. Osidak, P.A. Karalkin, M.S. Osidak, V.A. Parfenov, D.E. Sivogrivov, F. Pereira, A.A.
2 Gryadunova, E.V. Koudan, Y.D. Khesuani, C.V.A. capital Ka, S.I. Belousov, S.V.
3 Krasheninnikov, T.E. Grigoriev, S.N. Chvalun, E.A. Bulanova, V.A. Mironov, S.P.
4 Domogatsky, Viscoll collagen solution as a novel bioink for direct 3D bioprinting, *J Mater Sci*
5 *Mater Med* 30(3) (2019) 31.
- 6 [20] K.K. Moncal, V. Ozbolat, P. Datta, D.N. Heo, I.T. Ozbolat, Thermally-controlled
7 extrusion-based bioprinting of collagen, *J Mater Sci Mater Med* 30(5) (2019) 55.
- 8 [21] B.A. Nerger, P.T. Brun, C.M. Nelson, Microextrusion printing cell-laden networks of type
9 I collagen with patterned fiber alignment and geometry, *Soft Matter* 15(28) (2019) 5728-5738.
- 10 [22] S. Rhee, J.L. Puetzer, B.N. Mason, C.A. Reinhart-King, L.J. Bonassar, 3D Bioprinting of
11 Spatially Heterogeneous Collagen Constructs for Cartilage Tissue Engineering, *ACS*
12 *Biomater Sci Eng* 2(10) (2016) 1800-1805.
- 13 [23] R.V. Iozzo, L. Schaefer, Proteoglycan form and function: A comprehensive
14 nomenclature of proteoglycans, *Matrix Biol* 42 (2015) 11-55.
- 15 [24] M. Baniasadi, M. Minary-Jolandan, Alginate-Collagen Fibril Composite Hydrogel,
16 *Materials (Basel)* 8(2) (2015) 799-814.
- 17 [25] K. Gavenis, U. Schneider, U. Maus, T. Mumme, R. Muller-Rath, B. Schmidt-Rohlfing, S.
18 Andereya, Cell-free repair of small cartilage defects in the Goettinger minipig: which defect
19 size is possible?, *Knee Surg Sports Traumatol Arthrosc* 20(11) (2012) 2307-14.
- 20 [26] C.D. Reyes, A.J. García, Engineering integrin-specific surfaces with a triple-helical
21 collagen-mimetic peptide, *Journal of Biomedical Materials Research Part A* 65A(4) (2003)
22 511-523.
- 23 [27] S. Andereya, U. Maus, K. Gavenis, R. Muller-Rath, O. Miltner, T. Mumme, U. Schneider,
24 [First clinical experiences with a novel 3D-collagen gel (CaReS) for the treatment of focal
25 cartilage defects in the knee], *Z Orthop Ihre Grenzgeb* 144(3) (2006) 272-80.
- 26 [28] T. Efe, C. Theisen, S. Fuchs-Winkelmann, T. Stein, A. Getgood, M.B. Rominger, J.R.
27 Paletta, M.D. Schofer, Cell-free collagen type I matrix for repair of cartilage defects-clinical
28 and magnetic resonance imaging results, *Knee Surg Sports Traumatol Arthrosc* 20(10)
29 (2012) 1915-22.
- 30 [29] U. Schneider, B. Schmidt-Rohlfing, K. Gavenis, U. Maus, R. Mueller-Rath, S. Andereya,
31 A comparative study of 3 different cartilage repair techniques, *Knee Surg Sports Traumatol*
32 *Arthrosc* 19(12) (2011) 2145-52.
- 33 [30] K.F. Schuettler, J. Struwer, M.B. Rominger, P. Rexin, T. Efe, Repair of a chondral
34 defect using a cell free scaffold in a young patient--a case report of successful scaffold
35 transformation and colonisation, *BMC Surg* 13 (2013) 11.
- 36 [31] J. Zhu, L.J. Kaufman, Collagen I self-assembly: revealing the developing structures that
37 generate turbidity, *Biophys J* 106(8) (2014) 1822-31.

- 1 [32] S. Zhu, Q. Yuan, T. Yin, J. You, Z. Gu, S. Xiong, Y. Hu, Self-assembly of collagen-based
2 biomaterials: preparation, characterizations and biomedical applications, *J Mater Chem B*
3 6(18) (2018) 2650-2676.
- 4 [33] N. Latifi, M. Asgari, H. Vali, L. Mongeau, A tissue-mimetic nano-fibrillar hybrid injectable
5 hydrogel for potential soft tissue engineering applications, *Sci Rep* 8(1) (2018) 1047.
- 6 [34] C. Loebel, M. D'Este, M. Alini, M. Zenobi-Wong, D. Eglin, Precise tailoring of tyramine-
7 based hyaluronan hydrogel properties using DMTMM conjugation, *Carbohydr Polym* 115
8 (2015) 325-33.
- 9 [35] B. Hoyer, A. Bernhardt, A. Lode, S. Heinemann, J. Sewing, M. Klinger, H. Notbohm, M.
10 Gelinsky, Jellyfish collagen scaffolds for cartilage tissue engineering, *Acta Biomater* 10(2)
11 (2014) 883-92.
- 12 [36] M.S. Saravanan, J. Jayamani, G. Shanmugam, B. Madhan, High concentration of
13 propanol does not significantly alter the triple helical structure of type I collagen, *Colloid and*
14 *Polymer Science* 293(9) (2015) 2655-2662.
- 15 [37] K. Kar, P. Amin, M.A. Bryan, A.V. Persikov, A. Mohs, Y.H. Wang, B. Brodsky, Self-
16 association of collagen triple helix peptides into higher order structures, *J Biol Chem* 281(44)
17 (2006) 33283-90.
- 18 [38] B.R. Williams, R.A. Gelman, D.C. Poppke, K.A. Piez, Collagen fibril formation. Optimal in
19 vitro conditions and preliminary kinetic results, *J Biol Chem* 253(18) (1978) 6578-85.
- 20 [39] O.F. Gardner, M. Alini, M.J. Stoddart, Mesenchymal Stem Cells Derived from Human
21 Bone Marrow, *Methods Mol Biol* 1340 (2015) 41-52.
- 22 [40] C. Loebel, T. Stauber, M. D'Este, M. Alini, M. Zenobi-Wong, D. Eglin, Fabrication of cell-
23 compatible hyaluronan hydrogels with a wide range of biophysical properties through high
24 tyramine functionalization, *J Mater Chem B* 5(12) (2017) 2355-2363.
- 25 [41] R. Tognato, A.R. Armiento, V. Bonfrate, R. Levato, J. Malda, M. Alini, D. Eglin, G.
26 Giancane, T. Serra, A Stimuli-Responsive Nanocomposite for 3D Anisotropic Cell-Guidance
27 and Magnetic Soft Robotics, *Adv Funct Mater* 29(9) (2019) 1804647.
- 28 [42] C.E. Ayres, B.S. Jha, H. Meredith, J.R. Bowman, G.L. Bowlin, S.C. Henderson, D.G.
29 Simpson, Measuring fiber alignment in electrospun scaffolds: a user's guide to the 2D fast
30 Fourier transform approach, *J Biomater Sci Polym Ed* 19(5) (2008) 603-21.
- 31 [43] R. Farndale, D. Buttle, A. Barrett, Improved quantitation and discrimination of sulphated
32 glycosaminoglycans by use of dimethylmethylene blue, *Biochim Biophys Acta Gen Subj*
33 883(2) (1986) 173-177.
- 34 [44] J.A. Buckwalter, V.C. Mow, A. Ratcliffe, Restoration of Injured or Degenerated Articular
35 Cartilage, *J Am Acad Orthop Surg* 2(4) (1994) 192-201.

- 1 [45] D. Petta, A.R. Armiento, D. Grijpma, M. Alini, D. Eglin, M. D'Este, 3D bioprinting of a
2 hyaluronan bioink through enzymatic-and visible light-crosslinking, *Biofabrication* 10(4)
3 (2018) 044104.
- 4 [46] A. Frayssinet, D. Petta, C. Illoul, B. Haye, A. Markitantova, D. Eglin, G. Mosser, M.
5 D'Este, C. Helary, Extracellular matrix-mimetic composite hydrogels of cross-linked
6 hyaluronan and fibrillar collagen with tunable properties and ultrastructure, *Carbohydr Polym*
7 236 (2020) 116042.
- 8 [47] M. Binner, L.J. Bray, J. Friedrichs, U. Freudenberg, M.V. Tsurkan, C. Werner, Cell-
9 instructive starPEG-heparin-collagen composite matrices, *Acta Biomater* 53 (2017) 70-80.
- 10 [48] K.V. Nguyen-Ngoc, A.J. Ewald, Mammary ductal elongation and myoepithelial migration
11 are regulated by the composition of the extracellular matrix, *J Microsc* 251(3) (2013) 212-23.
- 12 [49] A.D. Nocera, R. Comin, N.A. Salvatierra, M.P. Cid, Development of 3D printed fibrillar
13 collagen scaffold for tissue engineering, *Biomed Microdevices* 20(2) (2018) 26.
- 14 [50] D.F. Duarte Campos, M. Rohde, M. Ross, P. Anvari, A. Blaeser, M. Vogt, C. Panfil, G.H.
15 Yam, J.S. Mehta, H. Fischer, P. Walter, M. Fuest, Corneal bioprinting utilizing collagen-
16 based bioinks and primary human keratocytes, *J Biomed Mater Res A* 107(9) (2019) 1945-
17 1953.
- 18 [51] D. Petta, D.W. Grijpma, M. Alini, D. Eglin, M. D'Este, Three-Dimensional Printing of a
19 Tyramine Hyaluronan Derivative with Double Gelation Mechanism for Independent Tuning of
20 Shear Thinning and Postprinting Curing, *ACS Biomater Sci Eng* 4(8) (2018) 3088-3098.
- 21 [52] A. Sundarakrishnan, H. Zukas, J. Coburn, B.T. Bertini, Z. Liu, I. Georgakoudi, L. Baugh,
22 Q. Dasgupta, L.D. Black, D.L. Kaplan, Bioengineered in Vitro Tissue Model of Fibroblast
23 Activation for Modeling Pulmonary Fibrosis, *ACS Biomater Sci Eng* 5(5) (2019) 2417-2429.
- 24 [53] H. Kim, J. Jang, J. Park, K.P. Lee, S. Lee, D.M. Lee, K.H. Kim, H.K. Kim, D.W. Cho,
25 Shear-induced alignment of collagen fibrils using 3D cell printing for corneal stroma tissue
26 engineering, *Biofabrication* 11(3) (2019) 035017.
- 27 [54] J. Lin, Y. Shi, Y. Men, X. Wang, J. Ye, C. Zhang, Mechanical Roles in Formation of
28 Oriented Collagen Fibers, *Tissue Eng Part B Rev* 26(2) (2020) 116-128.
- 29 [55] A. Kamada, A. Levin, Z. Toprakcioglu, Y. Shen, V. Lutz-Bueno, K.N. Baumann, P.
30 Mohammadi, M.B. Linder, R. Mezzenga, T.P.J. Knowles, Modulating the Mechanical
31 Performance of Macroscale Fibers through Shear-Induced Alignment and Assembly of
32 Protein Nanofibrils, *Small* 16(9) (2020) 1904190.
- 33 [56] M.K. Hausmann, P.A. Ruhs, G. Siqueira, J. Lauger, R. Libanori, T. Zimmermann, A.R.
34 Studart, Dynamics of Cellulose Nanocrystal Alignment during 3D Printing, *ACS Nano* 12(7)
35 (2018) 6926-6937.

- 1 [57] M. Kopf, D.F. Campos, A. Blaeser, K.S. Sen, H. Fischer, A tailored three-dimensionally
2 printable agarose-collagen blend allows encapsulation, spreading, and attachment of human
3 umbilical artery smooth muscle cells, *Biofabrication* 8(2) (2016) 025011.
- 4 [58] M. Betsch, C. Cristian, Y.Y. Lin, A. Blaeser, J. Schoneberg, M. Vogt, E.M. Buhl, H.
5 Fischer, D.F. Duarte Campos, Incorporating 4D into Bioprinting: Real-Time Magnetically
6 Directed Collagen Fiber Alignment for Generating Complex Multilayered Tissues, *Adv*
7 *Healthc Mater* 7(21) (2018) e1800894.
- 8 [59] Y. Yang, Z. Chen, X. Song, Z. Zhang, J. Zhang, K.K. Shung, Q. Zhou, Y. Chen,
9 Biomimetic Anisotropic Reinforcement Architectures by Electrically Assisted Nanocomposite
10 3D Printing, *Adv Mater* 29(11) (2017).
- 11 [60] L. Ouyang, R. Yao, Y. Zhao, W. Sun, Effect of bioink properties on printability and cell
12 viability for 3D bioplotting of embryonic stem cells, *Biofabrication* 8(3) (2016) 035020.
- 13 [61] I.L. Kim, S. Khetan, B.M. Baker, C.S. Chen, J.A. Burdick, Fibrous hyaluronic acid
14 hydrogels that direct MSC chondrogenesis through mechanical and adhesive cues,
15 *Biomaterials* 34(22) (2013) 5571-80.
- 16 [62] A.D. Doyle, N. Carvajal, A. Jin, K. Matsumoto, K.M. Yamada, Local 3D matrix
17 microenvironment regulates cell migration through spatiotemporal dynamics of contractility-
18 dependent adhesions, *Nat Commun* 6 (2015) 8720.
- 19 [63] T.L. Jenkins, D. Little, Synthetic scaffolds for musculoskeletal tissue engineering: cellular
20 responses to fiber parameters, *NPJ Regen Med* 4 (2019) 15.
- 21 [64] S. Yang, X. Shi, X. Li, J. Wang, Y. Wang, Y. Luo, Oriented collagen fiber membranes
22 formed through counter-rotating extrusion and their application in tendon regeneration,
23 *Biomaterials* 207 (2019) 61-75.
- 24 [65] R. Mohan, N. Mohan, D. Vaikkath, Hyaluronic Acid Dictates Chondrocyte Morphology
25 and Migration in Composite Gels, *Tissue Eng Part A* 24(19-20) (2018) 1481-1491.
- 26 [66] E. Amann, P. Wolff, E. Breel, M. van Griensven, E.R. Balmayor, Hyaluronic acid
27 facilitates chondrogenesis and matrix deposition of human adipose derived mesenchymal
28 stem cells and human chondrocytes co-cultures, *Acta Biomater* 52 (2017) 130-144.
- 29 [67] Y. Wang, Y. Xiao, S. Long, Y. Fan, X. Zhang, Role of N-Cadherin in a Niche-Mimicking
30 Microenvironment for Chondrogenesis of Mesenchymal Stem Cells In Vitro, *ACS*
31 *Biomaterials Science & Engineering* (2020).
- 32 [68] H. Rogan, F. Ilagan, F. Yang, Comparing Single Cell Versus Pellet Encapsulation of
33 Mesenchymal Stem Cells in Three-Dimensional Hydrogels for Cartilage Regeneration,
34 *Tissue Eng Part A* 25(19-20) (2019) 1404-1412.
- 35 [69] B.D. Markway, G.K. Tan, G. Brooke, J.E. Hudson, J.J. Cooper-White, M.R. Doran,
36 Enhanced chondrogenic differentiation of human bone marrow-derived mesenchymal stem
37 cells in low oxygen environment micropellet cultures, *Cell Transplant* 19(1) (2010) 29-42.

- 1 [70] X. Jiang, X. Huang, T. Jiang, L. Zheng, J. Zhao, X. Zhang, The role of Sox9 in collagen
2 hydrogel-mediated chondrogenic differentiation of adult mesenchymal stem cells (MSCs),
3 *Biomater Sci* 6(6) (2018) 1556-1568.
- 4 [71] C.G. Pfeifer, A. Berner, M. Koch, W. Krutsch, R. Kujat, P. Angele, M. Nerlich, J. Zellner,
5 Higher Ratios of Hyaluronic Acid Enhance Chondrogenic Differentiation of Human MSCs in a
6 Hyaluronic Acid-Gelatin Composite Scaffold, *Materials (Basel)* 9(5) (2016).
- 7 [72] V. Moulisova, S. Poveda-Reyes, E. Sanmartin-Masia, L. Quintanilla-Sierra, M.
8 Salmeron-Sanchez, G. Gallego Ferrer, Hybrid Protein-Glycosaminoglycan Hydrogels
9 Promote Chondrogenic Stem Cell Differentiation, *ACS Omega* 2(11) (2017) 7609-7620.
- 10 [73] J. Yang, Y. Liu, L. He, Q. Wang, L. Wang, T. Yuan, Y. Xiao, Y. Fan, X. Zhang, Icaritin
11 conjugated hyaluronic acid/collagen hydrogel for osteochondral interface restoration, *Acta*
12 *Biomater* 74 (2018) 156-167.

1 6 Figure captions

2 **Figure 1: 3D bioprinting as a tool to produce microscopic anisotropic scaffolds.** Biomaterial and
3 bioink were prepared by mixing neutralized Col 1 (5 mg/ml) isolated from rat tails with tyramine
4 modified HA (THA, 25 mg/ml). Neutralized Col 1 was mixed with THA for enzymatic crosslinking either
5 cell free or containing hMSC cell micro pellets. The Col 1 microstructure was investigated after 3D
6 printing and compared to casted, isotropic samples with different microscopic techniques (Second
7 Harmonic Generation SHG imaging and confocal microscopy). Cell instructive properties were
8 analyzed after in vitro culture on cell migration and attachment.

9
10 **Figure 2: Collagen (Col 1) fibrils distribution in THA hydrogel and rheological properties.** A)
11 Visualization of Col 1 fibrils within Col 1 hydrogel and B) THA-Col 1 hydrogels using confocal imaging
12 (immunofluorescent staining for Col 1) and C-D) SHG imaging (no labelling), respectively. Both
13 techniques illustrate homogenous distribution of Col 1 fibrils (scale bar 100 μm). E) Turbidity
14 measurement of THA-Col 1 demonstrated Col 1 fibril formation in composite dependent on Col 1
15 content. The more Col 1 is present in composite the higher the absorbance at 313 nm over time with
16 maximum values for Col 1 only. F) Flow curve (viscosity as function of shear rate) demonstrate shear
17 thinning behavior of THA, THA-Col 1 and neutralized Col 1 marked by decreasing viscosity with
18 increasing shear rate. Col 1 (pH7, 5 mg/ml) showed lower viscosity compared to THA (25 mg/ml) and
19 THA-Col 1. Acidic Col 1 (pH 4, 5 mg/ml) lacks shear-thinning behavior with a constant viscosity over
20 range of tested shear rate. G) Rheological characterization (Amplitude sweep, 1Hz) to evaluate
21 mechanical properties of biomaterial ink by means of storage (G') and loss (G'') modulus of THA-Col
22 1 and THA after enzymatic crosslinking. Storage modulus increases in composite compared to THA.

23
24 **Figure 3: Cell instructive properties of THA-Col 1 addressing hMSC migration and cell**
25 **attachment.** A) Confocal images of actin filament stained hMSC micro pellets embedded in THA-Col 1
26 (THA-Col 1, 25 mg/ml 1:1 Col 1 5 mg/ml), THA (25 mg/ml) and Col 1 (5 mg/ml) at day 0, day 3 and
27 after 8 days culture. Migration of hMSC was seen for THA-Col 1 and Col 1 but not in THA. Col 1
28 hydrogel was shrinking over time and formed a small pellet of less than 2 mm in diameter (Scale bar

1 100 μm). B) Area of cell migration and C) migration length was higher in Col 1 compared to THA-Col 1
2 increasing over time. Quantification of migration area and migration length. ** $p < 0.01$, *** $p < 0.001$.

3

4 **Figure 4: Chondrogenic differentiation potential of hMSC embedded in THA-Col 1 compared to**
5 **hMSC pellet culture.** A) Gene expression analysis relative to hMSC pellet or hMSC embedded in
6 THA-Col 1 hydrogel (TC MSC) control at day 0 for Col 1 (COL 1A1), Col II (COL 2A1), aggrecan
7 (ACAN), SOX9 and RunX2. Increase in all chondrogenic related genes with minor changes for SOX9
8 and RunX2. B) Relative gene expression ratio of Col 2 to Col 1 at day 21. No statistical differences
9 resulted for all PCR data shown beside for Col2/Col 1 ratio. * $p < 0.05$ C) Quantification of proteoglycans
10 (GAG/sample) including total amount of GAGs released into the media supernatant and GAGs
11 retained in the sample at day 21. D) GAG/DNA increased over time from day 0 to day 21 for MSC
12 pellet and THA-Col 1 MSC. **** $p < 0.0001$. E) Safranin O staining to visualize proteoglycans in ECM
13 after 21 days in vitro culture at two magnifications for MSC pellet and F) MSC embedded in THA-Col 1
14 hydrogel (THA-Col 1 MSC) (scale bar 100 μm).

15

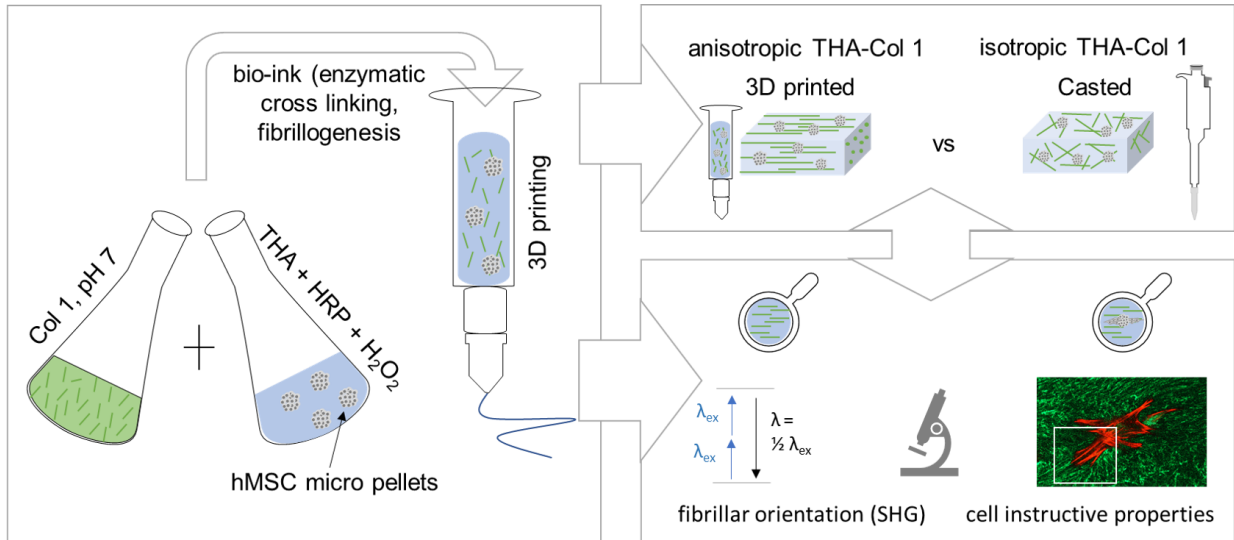
16 **Figure 5: 3DP as tool to align Col 1 fibers and produce microscopically anisotropic scaffolds.**

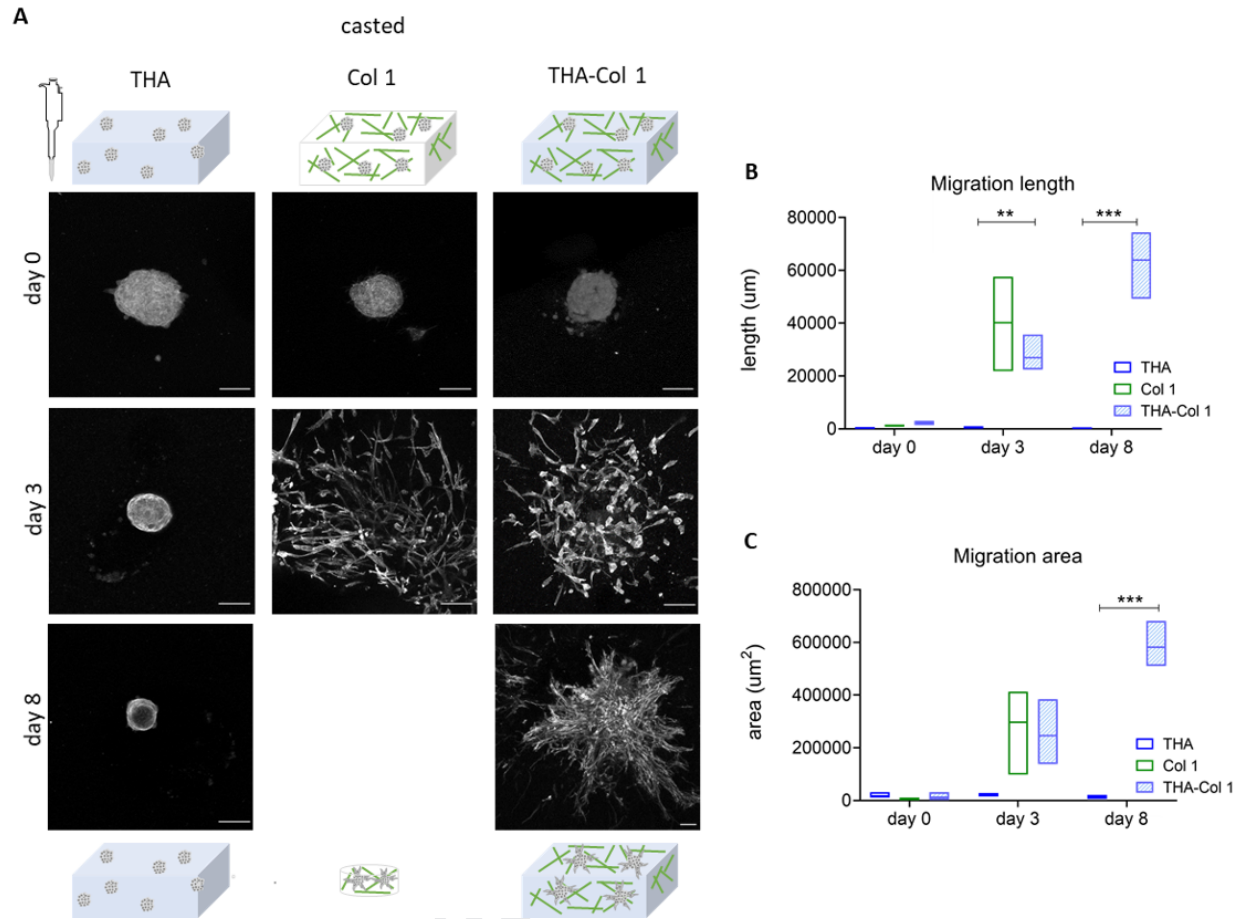
17 A) Confocal microscopy of immunofluorescent staining against Col 1 and C) SHG images demonstrate
18 anisotropic fibers in THA-Col 1 biomaterial ink (scale bar 100 μm). Unidirectional orientation of parallel
19 Col 1 fibers aligning along the printing direction (white arrow indicated printing direction). B, D) Bar
20 diagrams (mean values \pm standard deviation) display the quantification of fiber alignment in casted Col
21 1, casted THA-Col 1 (ID 1.0 mm) and printed THA-Col 1 (15G: ID 1.36 mm, 0.25" cylindrical needle)
22 from images acquired either with confocal microscope (B, green) or SHG (D, blue). Independently of
23 microscopical method the printed THA-Col 1 samples resulted in unidirectional orientation which was
24 more random for casted THA-Col 1 and Col 1. White arrow in the bar diagram indicate the peak width
25 at a normalized grey value of 0.5. E) Schematic illustration of Col 1 fiber alignment in articular
26 cartilage. F) Polarized light image of articular cartilage illustrating horizontal fibers in superficial zone
27 (SZ) and vertical orientation in deep zone (DZ) (scale bar 50 μm). G) Macroscopic image of complex
28 micro structured scaffold (1.4 x 1.6 cm in size, 18G: ID 0.84 mm, 0.25" cylindrical needle) mimicking
29 collagen fiber orientation present in articular cartilage (scale bar 500 μm). H) Confocal images of
30 immunofluorescent labelled Col 1 mimicking hierarchical fiber orientation in articular cartilage with

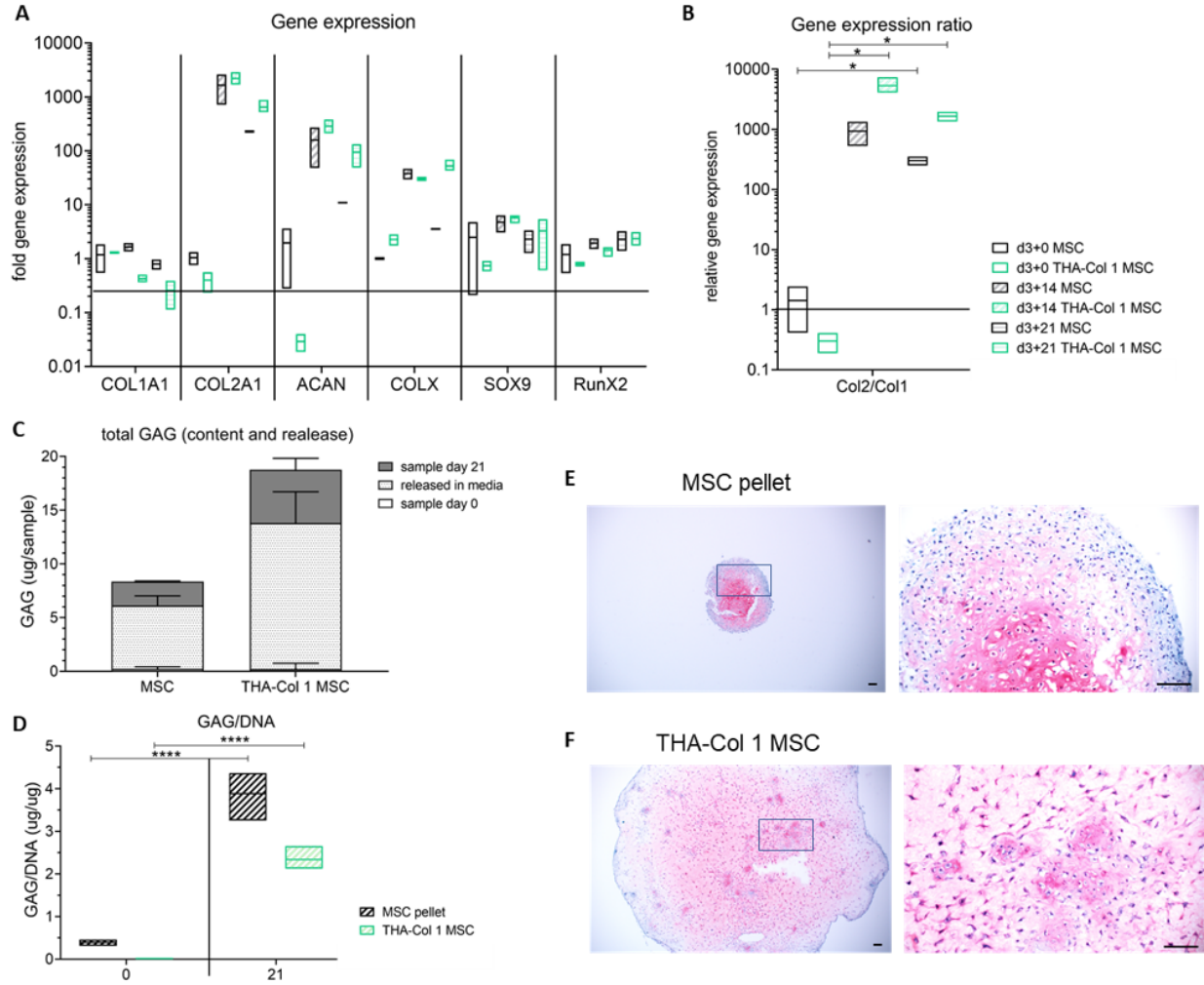
1 parallel horizontal fibers in the SZ, more isotropic fibers in the middle zone (MZ) and parallel vertical
2 fibers in the DZ (scale bar 50 μm).

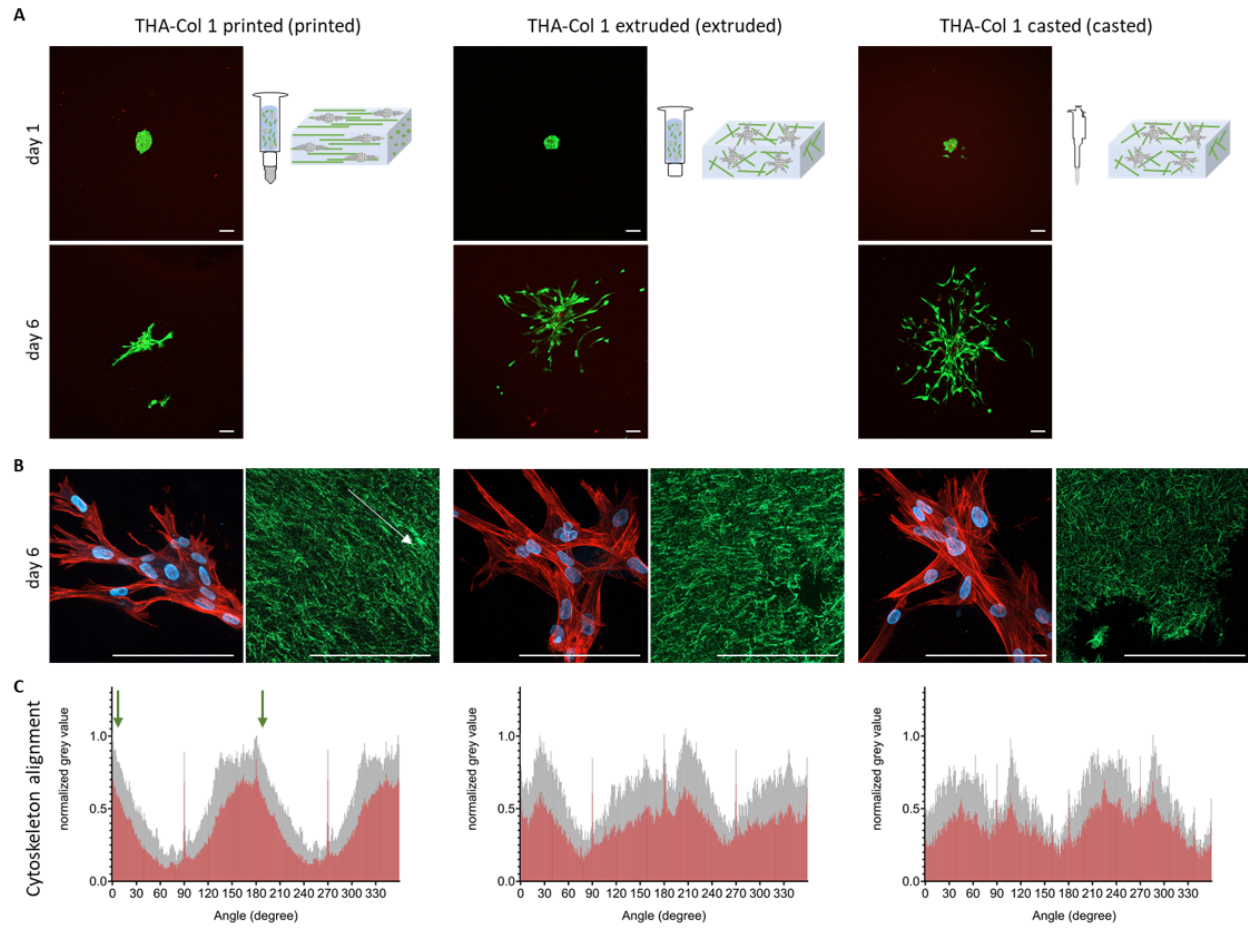
3

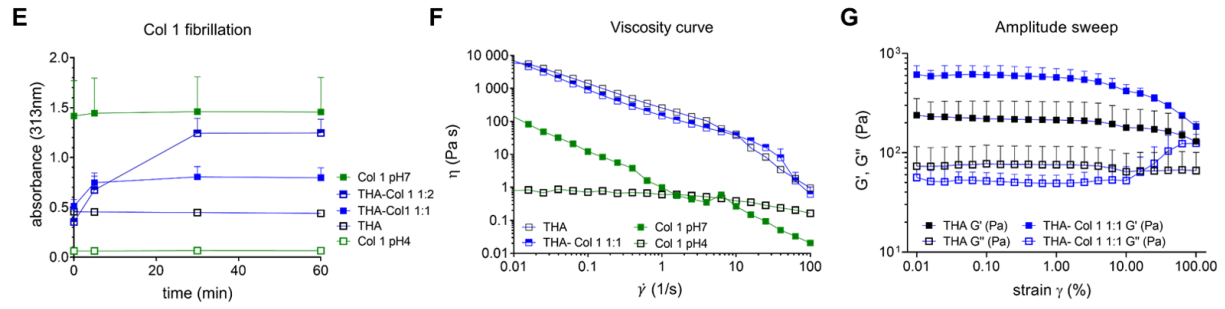
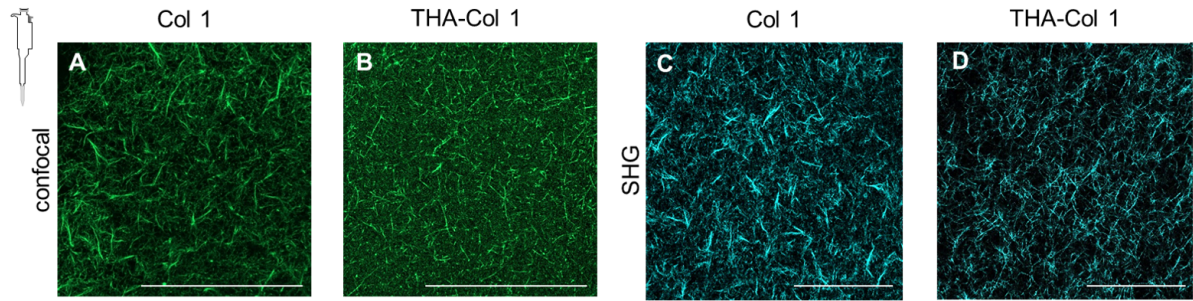
4 **Figure 6: Viability (Live/dead staining) and phalloidin staining of hMSC micro pellets in THA-**
5 **Col 1 hydrogel.** A) Representative images of live/dead staining at day 1 and day 6 showing living
6 cells in green with few dead cells in red (Scale bar 100 μm). Bio-ink was either printed with 15G (ID
7 1.36 mm) cylindrical needle, extruded from 3CC cartridge (ID 2.4 mm) or pipetted with CP100 positive
8 displacement pipette (ID 1.0 mm). B) MAX z-projection of hMSCs after 6 days of culture in THA-Col 1
9 demonstrating unidirectional actin filaments/cell cytoskeleton (in red) along the Col 1 (green) direction
10 of printed samples (white arrow indicates printing direction) and cell nuclei (blue). In extruded and
11 casted samples cells migrated random in the bioink (scale bar 100 μm). C) Orientation of cytoskeleton
12 of hMSCs embedded in THA-Col 1 printed, extruded and casted displaying the mean values in red
13 with standard deviation in grey. More unidirectional alignment with smaller peak width of cytoskeleton
14 resulted for 15G printed THA-Col 1 compared to the two other groups. Green arrow in the graph of
15 printed sample indicates the printing direction.

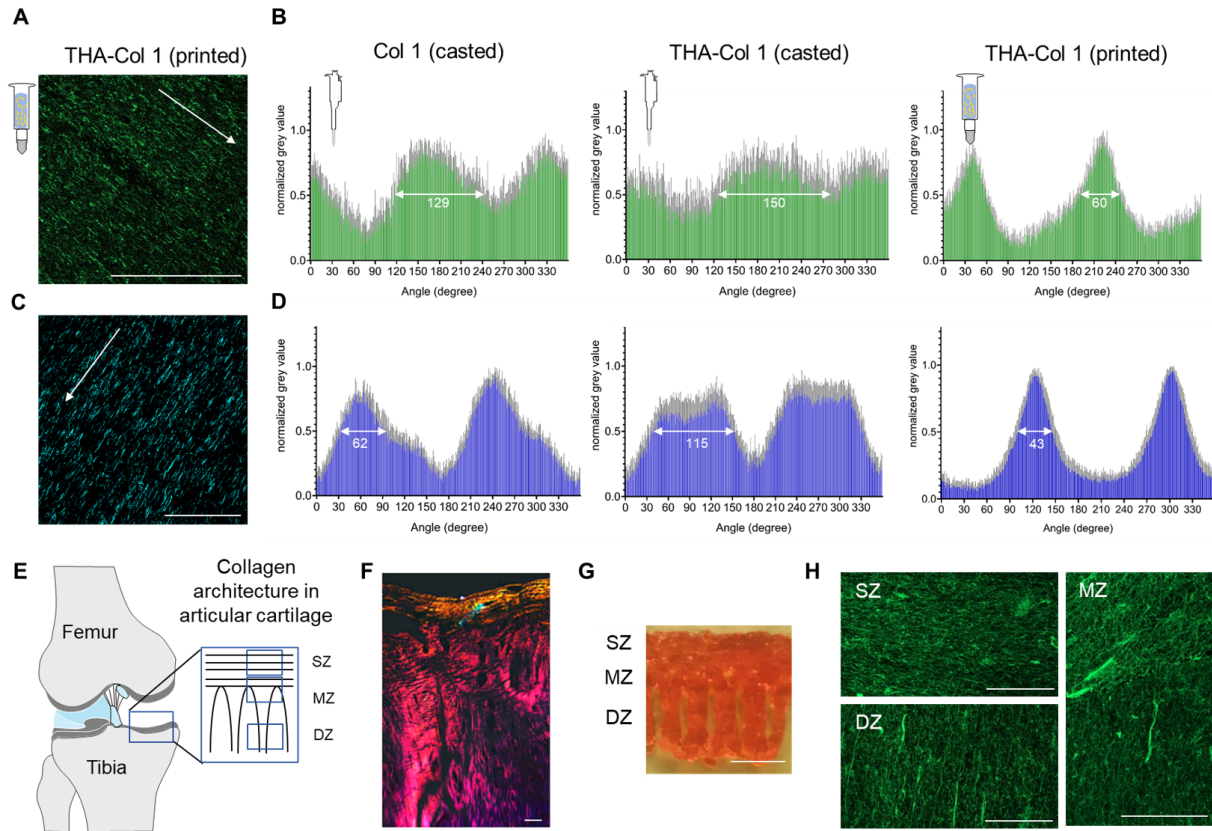












Highlights

- Tissue mimetic collagen I - hyaluronan bioink
- 3D printing to control microscopic alignment of fibrillar collagen
- Control over collagen fibril orientation to modulate cell alignment
- Pro-chondrogenic potential of composite biomaterial

Journal Pre-proof

Declaration of interests

The authors declare that they have no known competing financial interests or personal relationships that could have appeared to influence the work reported in this paper.

The authors declare the following financial interests/personal relationships which may be considered as potential competing interests:

On behalf of the Authors, the corresponding author Dr. Matteo D'Este



Journal Pre-proof